



This is a repository copy of *The m6A-methylase complex recruits TREX and regulates mRNA export.*

White Rose Research Online URL for this paper:
<http://eprints.whiterose.ac.uk/135762/>

Version: Published Version

Article:

Lesbirel, S., Viphakone, N., Parker, M. et al. (4 more authors) (2018) The m6A-methylase complex recruits TREX and regulates mRNA export. *Scientific Reports*, 8 (1). 13827. ISSN 2045-2322

<https://doi.org/10.1038/s41598-018-32310-8>

© The Author(s) 2018. This article is licensed under a Creative Commons Attribution 4.0 International License, which permits use, sharing, adaptation, distribution and reproduction in any medium or format, as long as you give appropriate credit to the original author(s) and the source, provide a link to the Creative Commons license, and indicate if changes were made. The images or other third party material in this article are included in the article's Creative Commons license, unless indicated otherwise in a credit line to the material. If material is not included in the article's Creative Commons license and your intended use is not permitted by statutory regulation or exceeds the permitted use, you will need to obtain permission directly from the copyright holder. To view a copy of this license, visit <http://creativecommons.org/licenses/by/4.0/>.

Reuse

This article is distributed under the terms of the Creative Commons Attribution (CC BY) licence. This licence allows you to distribute, remix, tweak, and build upon the work, even commercially, as long as you credit the authors for the original work. More information and the full terms of the licence here:
<https://creativecommons.org/licenses/>


Takedown

If you consider content in White Rose Research Online to be in breach of UK law, please notify us by emailing eprints@whiterose.ac.uk including the URL of the record and the reason for the withdrawal request.



eprints@whiterose.ac.uk
<https://eprints.whiterose.ac.uk/>

SCIENTIFIC REPORTS



OPEN

The m⁶A-methylase complex recruits TREX and regulates mRNA export

Simon Lesbirel, Nicolas Viphakone, Matthew Parker, Jacob Parker, Catherine Heath, Ian Sudbery & Stuart A. Wilson

N⁶-methyladenosine (m⁶A) is the most abundant internal modification of eukaryotic mRNA. This modification has previously been shown to alter the export kinetics for mRNAs though the molecular details surrounding this phenomenon remain poorly understood. Recruitment of the TREX mRNA export complex to mRNA is driven by transcription, 5' capping and pre-mRNA splicing. Here we identify a fourth mechanism in human cells driving the association of TREX with mRNA involving the m⁶A methylase complex. We show that the m⁶A complex recruits TREX to m⁶A modified mRNAs and this process is essential for their efficient export. TREX also stimulates recruitment of the m⁶A reader protein YTHDC1 to the mRNA and the m⁶A complex influences the interaction of TREX with YTHDC1. Together our studies reveal a key role for TREX in the export of m⁶A modified mRNAs.

The transport of mRNA from the nucleus to the cytoplasm represents a key step in the eukaryotic gene expression pathway. mRNA export is closely coupled with capping, splicing and 3' end processing of primary transcripts¹. The integration of RNA processing and export ensure high fidelity in the gene expression process and competition between export and surveillance factors determines whether mRNAs are exported or degraded². The major complex involved in mRNA export is TREX which has 14 known subunits¹. TREX triggers the recruitment of the NXF1:NXT1 heterodimer which is required for translocation of mRNA from its site of transcription through the nuclear pore to the cytoplasm. This is achieved by adaptor (ALYREF) and co-adaptor (CHTOP and THOC5) subunits within TREX which drive NXF1 into a conformation allowing a stable interaction with mRNA^{3,4}. Additional adaptor proteins which bind and recruit NXF1 to the mRNP have been identified most notably SR proteins^{5,6}.

Beyond RNA processing, a number of other regulatory processes have been implicated in mRNA export control including methylation of RNA, though the molecular mechanisms are unclear. The N⁶ methyladenosine modification (m⁶A) is the most common internal methylation event in mRNA⁷. Recent work indicates that it is persistent from birth to degradation of target mRNA under steady state conditions and its addition reduces the half life of its target mRNAs⁸. m⁶A influences a number of other processes including pre-mRNA splicing, alternative polyadenylation and translation^{9,10}. Genome-wide analyses using the technique of m⁶A-seq^{11,12} and more recently cross-linking immunoprecipitation (CLIP)¹³ have revealed a distinctive landscape of m⁶A modifications on mRNAs with peaks in long internal exons and 3' UTRs. These peaks are enriched in an RRACU consensus sequence. The heterodimeric METTL3 and METTL14 complex is responsible for the catalytic addition of the m⁶A modification upon target RNAs, often referred to as “writers”. Two further regulatory members of the m⁶A complex, WTAP and KIAA1429, are responsible for the targeting and formation of an active m⁶A complex^{14,15}. RBM15 and RBM15B bind the methylase complex and recruit it to specific sites in mRNA¹⁶. Notably both RBM15 and RBM15B have been implicated in mRNA export control^{17,18}. ZC3H13 is the most recently discovered member of the m⁶A complex which bridges the interaction between RBM15 and WTAP¹⁹ and maintains the nuclear localisation of the m⁶A complex²⁰.

The “reader proteins” recognise and bind the m⁶A modification and include cytoplasmic YTHDF1, 2, 3^{21,22}, nuclear YTHDC1²³, and several hnRNP proteins including HNRNPC which alters splicing decisions²⁴ and HNRNPA2B1 which regulates miRNA processing²⁵. The cytoplasmic reader proteins play roles in translation and mRNA stability^{22,26}. The nuclear reader protein, YTHDC1, has been implicated in splicing control²⁷ and

Sheffield Institute For Nucleic Acids (SInFoNiA), Department of Molecular Biology and Biotechnology, University of Sheffield, Firth Court Western Bank, Sheffield, S10 2TN, UK. Correspondence and requests for materials should be addressed to S.A.W. (email: stuart.wilson@sheffield.ac.uk)

transcriptional silencing of XIST¹⁶. YTHDC1 also plays a role in the control of mRNA export where it has been proposed to work in conjunction with SRSF3 to promote export of selected transcripts²⁸.

A further connection between the m⁶A machinery and mRNA export was observed following depletion of writer METTL3. This led to an alteration in the circadian clock through altered export kinetics for key mRNAs involved in this process²⁹, though the molecular mechanisms involved were not described. Finally, evidence of a connection between mRNA export and m⁶A comes from a class of proteins known as “erasers” (ALKBH5 and FTO) that can remove the modification. Both are members of the same ALKB subfamily of Fe(II)/2-oxoglutarate dioxygenases. FTO preferentially recognises N⁶-2'-O-dimethyladenosine (m⁶A_m) located adjacent to the mRNA m⁷G cap and this modification increases mRNA stability³⁰. ALKBH5 is located in nuclear speckles in common with mRNA splicing and export factors and its loss is reported to lead to increased cytoplasmic poly(A)⁺ RNA signal, suggesting an alteration in mRNA export control though again the molecular mechanisms involved are unclear³¹.

In this study we reveal how the m⁶A machinery exerts control on mRNA export via TREX. The m⁶A writer complex recruits TREX to specific mRNAs and TREX stimulates recruitment of YTHDC1 to the mRNP. Knockdown of the m⁶A writer complex also stimulates TREX interactions with YTHDC1. NXF1 associates with both TREX and YTHDC1 indicating they collaborate to drive efficient export of transcripts subject to m⁶A control.

Results

TREX associates with the m⁶A methyltransferase complex. To explore the connection between the m⁶A modification and mRNA export, we immunoprecipitated subunits of the m⁶A complex and assessed their interaction with TREX in the presence of RNase A, to disrupt interactions bridged by RNA (Fig. 1A,B). Multiple TREX subunits (ALYREF, UAP56, THOC5, CHTOP) co-immunoprecipitated (co-IP) with all four subunits of the core m⁶A complex (WTAP, METTL3, METTL14, KIAA1429). In contrast, HNRNPA1 did not, indicating that RNase A treatment prevented co-IP of general mRNP binding proteins. To further investigate these interactions we knocked down KIAA1429 using RNAi (Fig. 1C), carried out a WTAP IP and examined the impact on binding partners (Fig. 1D). Depletion of KIAA1429 significantly reduced the levels of METTL3 associated with WTAP, indicating KIAA1429 is important to maintain integrity of the core m⁶A complex. Furthermore, KIAA1429 RNAi led to reduced levels of TREX subunits associated with WTAP. However, the combined knockdown of WTAP and KIAA1429, did not disrupt the association of METTL3 with ALYREF (Fig. 1E). Therefore, the reduced levels of TREX associated with WTAP following KIAA1429 RNAi most likely reflect a reduced association of WTAP with METTL3 in that context. Whilst the levels of TREX subunits in the cell were unaffected by KIAA1429 RNAi, the levels of WTAP protein increased significantly (Fig. 1D, see inputs) as reported previously³², suggesting the cells attempts to compensate for KIAA1429 loss with increased WTAP levels. Together these results indicate that TREX associates with the m⁶A methylase complex.

The m⁶A methyltransferase complex regulates nuclear export of transcripts. Given the association of the m⁶A machinery with TREX, we investigated the functional consequences of this interaction. We focussed our analysis on KIAA1429 and WTAP since subcellular fractionation showed they were associated with the chromatin and nucleoplasmic fractions, similar to TREX subunits (Fig. S1A). RNAi mediated knockdown of KIAA1429, WTAP, or KIAA1429 + WTAP gave no detectable mRNA export block using oligo (dT) fluorescence *in situ* hybridisation (FISH) (Fig. S1B). We reasoned that this may be because only a fraction of the transcriptome is subject to m⁶A control¹¹. Therefore, we examined the nucleocytoplasmic distribution of selected transcripts following individual RNAi of KIAA1429 or WTAP using RT-qPCR. Transcripts were selected for analysis by cross referencing WTAP CLIP³³, YTHDC1 CLIP²³ and m⁶A RIPseq¹³. By comparing all three data sets we identified methylated transcripts bound by WTAP or YTHDC1 or both (Table S1). TAF7 was chosen as a methylated intronless transcript, negating any splicing defect we may have observed. PTPN12 and DICER contain large internal m⁶A modified exons^{11,13}. The transcripts GSTP1, MC1R and SYMPK were chosen as negative controls since they did not appear in our filtered list of methylated transcripts. We examined the nuclear/cytoplasmic ratio for the selected transcripts following single knockdown of either KIAA1429 or WTAP but did not see any significant differences (Fig. S2).

Since we had observed that KIAA1429 knockdown led to increased levels of WTAP protein, we reasoned that such a compensatory mechanism may mask any defects in mRNA export. We have observed similar compensatory mechanisms previously masking mRNA export defects for subunits of the TREX mRNA export complex³⁴. Therefore, we examined the impact of a combined knockdown of WTAP and KIAA1429 on the nucleocytoplasmic distribution of selected mRNAs. siRNA treatment led to robust knockdown of both WTAP and KIAA1429 (Fig. 2A), but the reduction in the levels of these proteins did not impact on METTL3 levels. Depletion of WTAP and KIAA1429 led to a clear increase in the nuclear/cytoplasmic ratio of the spliced and intronless RNAs selected for their binding to the m⁶A complex. In contrast, transcripts with no evidence for association with this complex (GSTP1 and SYMPK), showed no significant alteration in their nuclear/cytoplasmic ratios. These data suggest that the m⁶A methylation machinery is required for efficient export of transcripts it associates with.

As TREX associates with the m⁶A methylase complex we considered that the block in mRNA export observed following WTAP/KIAA1429 RNAi might be due to inefficient loading of TREX onto mRNAs recognised by the m⁶A complex. To test this we used RNA immunoprecipitation (RIP) combined with RT-qPCR to measure the amount of mRNAs associated with the TREX subunits ALYREF and DDX39A/B (Fig. 2C,D). WTAP/KIAA1429 knockdown led to a drastic reduction in the levels of selected transcripts associated with TREX subunits ALYREF and DDX39A/B, but had no impact on the levels of the control GSTP1 mRNA bound to these proteins. For both DICER1 and PTPN12, chosen as they have long internal exons containing m⁶A sites¹¹, the recruitment of ALYREF was also disrupted in regions of the mRNA not reported to have m⁶A sites (Fig. 2C). This suggests that

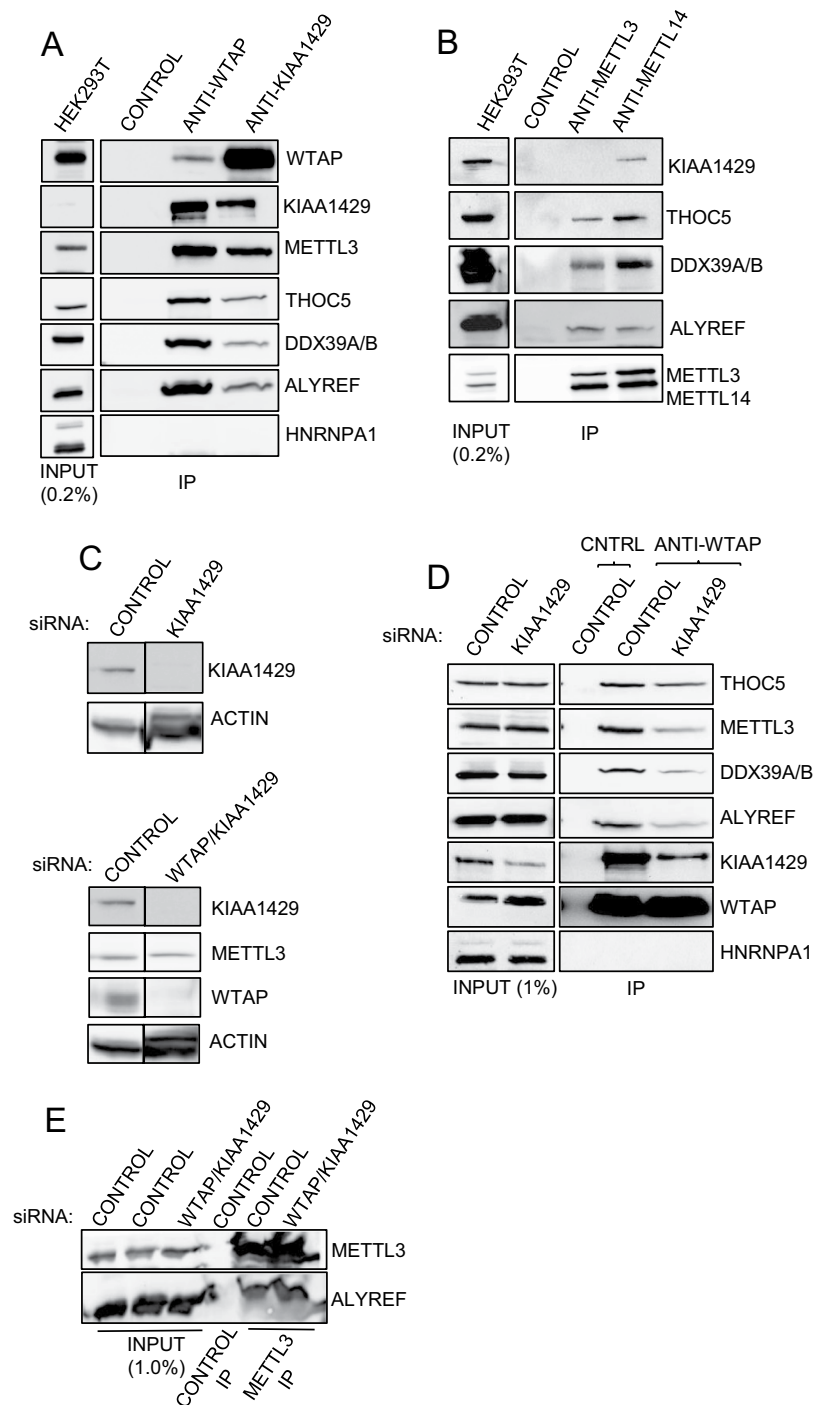


Figure 1. The TREX complex associates with the m^6A methyltransferase complex. **(A)** WTAP and KIAA1429 co-IP/Western analysis with TREX complex subunits. CONTROL antibody was anti-FLAG throughout the study. Antibodies used for IP are shown above the panels and antibodies used for detection on the right hand side of panels throughout the study. **(B)** METTL3/METTL14 Co-IP/Western with TREX subunits. **(C)** Western analysis showing efficient depletion of KIAA1429 by RNAi (upper panel). Combined KIAA1429 and WTAP siRNA treatment resulted in substantial knockdown of both proteins (lower panel). **(D)** WTAP Co-IP/Western analysis in a KIAA1429 siRNA background with the indicated TREX and m^6A machinery subunits. **(E)** METTL3 co-IP/Western analysis with ALYREF. METTL3 antibody was used for the IP. All Co-IP analysis presented in the paper were carried out in the presence of RNase A. Where separate panels are shown for same the protein in Western blots, these are all taken from the same blot at the same exposure. Full size blots are displayed in Supplementary Information.

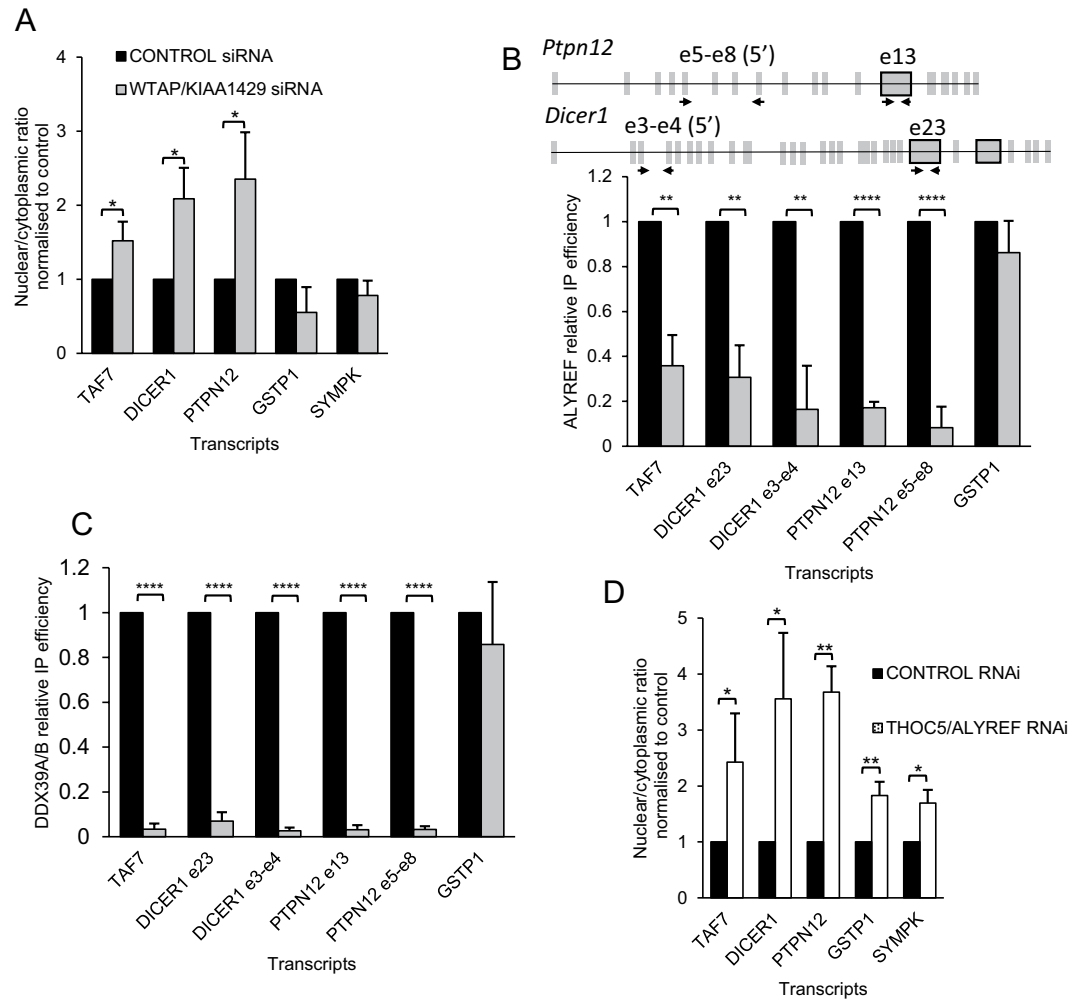


Figure 2. Co-knockdown of KIAA1429 and WTAP results in an export block for methylated transcripts. (A) qRT-qPCR analysis of m⁶A modified (TAF7 (intronless), DICER1, PTPN12 (spliced) and non-m⁶A modified mRNAs (GSTP1, SYMPK). The nuclear/cytoplasmic ratios normalised to control siRNA treated cells are shown. (B) ALYREF RNA immunoprecipitation (RIP) analysis by RT-qPCR are shown together with the positions of primers used on the long internal exon genes. Long internal exons with reported m⁶A sites¹¹ have a black outline. (C) DDX39A/B RIP analysis by RT-qPCR. (D) RT-qPCR analysis the nuclear/cytoplasmic ratios for selected transcripts following THOC5/ALYREF combined RNAi. RT-qPCR results throughout the paper represent the averages from 3 independent experiments with standard deviations presented.

either additional m⁶A sites are present in these mRNAs which have thus far eluded detection or alternatively that loss of ALYREF or UAP56/DDX39B at a single site on the mRNA has a propagative effect, leading to disruption of additional binding sites for these proteins on the mRNP. Double RNAi of ALYREF/THOC5 which disables TREX³⁴, led to a robust increase in the nuclear-cytoplasmic ratio for transcripts known to carry the m⁶A modification (Fig. 2E). Thus establishing that mRNAs dependent on WTAP/KIAA1429 for efficient export, also require TREX. Together these data show that the m⁶A methylase complex association with certain mRNAs leads to stable binding of TREX to those mRNAs and subsequent export.

Global analysis of WTAP/KIAA1429 knockdown on mRNA export. To extend our studies transcriptome-wide we carried out RNA-seq analysis of nuclear and cytoplasmic RNA fractions derived from cells depleted for both WTAP and KIAA1429. These studies identified 301 mRNAs whose nuclear/cytoplasmic ratio increased indicative of an mRNA export block and 111 mRNAs with a decreased nuclear/cytoplasmic ratio (Fig. 3A). Further investigation of the mRNAs with a decreased nuclear/cytoplasmic ratio revealed that 70% of them displayed a reduction in their nuclear levels and a concomitant increase in their cytoplasmic levels (Fig. S3D,E), suggesting that they are more exported. The average size of the effect on these mRNAs was much smaller than the effect on mRNAs with increased nuclear/cytoplasmic ratio (Fig. S3C,F) and these mRNAs had only a weak enrichment for genes previously reported to be methylated (1.5x enrichment, Fig. S3E). This suggests that the change to these cytoplasmically accumulating mRNAs could be an indirect effect. However, we did note an enrichment for genes annotated with the GO terms “endoplasmic reticulum” (2.9x enrichment,

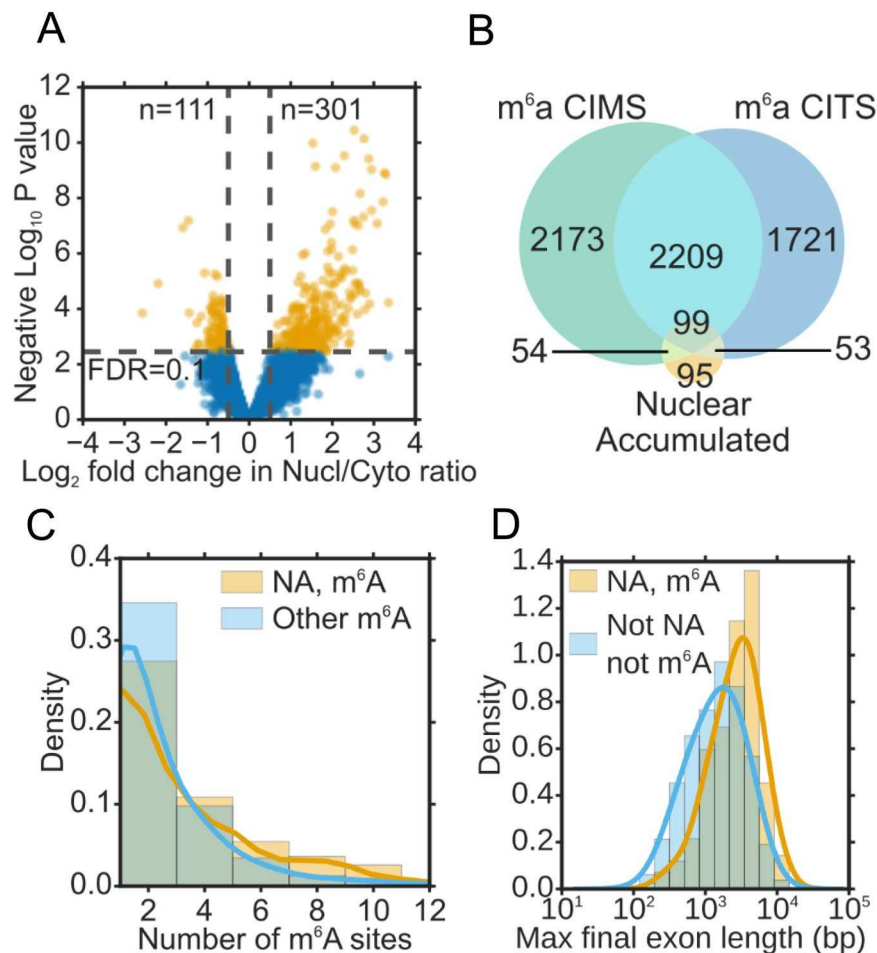


Figure 3. Global pattern of mRNA distribution following WTAP/KIAA1429 knockdown. **(A)** Volcano plot showing log₂ fold change in nuclear/cytoplasmic ratio in WTAP/KIAA1429 knockdown vs. control RNAi, determined by RNA-seq (n = 3). A fold change of 0.5 and an FDR of 0.1 were used to identify significantly differentially localised genes. **(B)** Overlap of nuclear accumulating genes with methylated genes, as determined by m⁶A iCLIP (miCLIP)⁵². Genes were considered to be methylated if they contained one or more miCLIP peaks within an exonic region of the gene. CIMS (cross linking induced mutation site) and CITS (crosslinking-induced truncation sites) are two alternative ways of identifying m⁶A sites as described in⁵². **(C)** Number of m⁶A sites in exonic regions per gene for nuclear accumulating (NA) methylated genes, vs. other methylated genes. **(D)** Length of the longest final exon per gene (log₁₀ scale) for NA methylated genes vs. non-NA non-methylated genes.

q-value = 0.008) and “extracellular region” (2.0x enrichment, q-value = 0.002). This is consistent with reports that mRNAs for some secreted proteins use an alternate export mechanism³⁵. Focussing on the mRNAs with an increased nuclear/cytoplasmic ratio, we found a strong overlap between this group and mRNAs previously reported to have m⁶A methylation sites (206/301 genes) (Fig. 3B). Moreover, gene products which displayed an mRNA export block had higher numbers of reported methylation sites than other methylated gene products which did not show nuclear accumulation (Fig. 3C). The methylated transcripts which showed nuclear accumulation also had longer final exons on average than non-methylated transcripts which did not show an export block (Fig. 3D). Consistent with an export block, we noted that 86% of mRNAs with an increased nuclear/cytoplasmic ratio, displayed increased nuclear and decreased cytoplasmic mRNA levels (Fig. S3A,B).

Since TREX deposition and mRNA export are coupled with splicing, we examined to what extent knockdown of WTAP/KIAA1429 altered splicing using the RNA-seq datasets. We looked at the frequency of retention of three classes of introns: constitutive, annotated retained and alternative (Fig. 4A). Retention of constitutive introns was detected in approximately 6% of gene products, whereas annotated retained and alternative introns showed much lower increases. These data indicate that WTAP and KIAA1429 are required for correct splicing of some mRNAs as reported previously^{10,36}. We examined the overlap between those gene products with retained introns and those which are reported to be methylated and found that 533 gene products with retained introns are reported to be methylated (Fig. 4B). The remaining 593 gene products with intron retention are not reported as methylated, but this may be due to poor sensitivity in detection of this modification in certain mRNAs. Alternatively, this may point to a role for these proteins in splicing not connected with their ability to trigger the m⁶A modification.

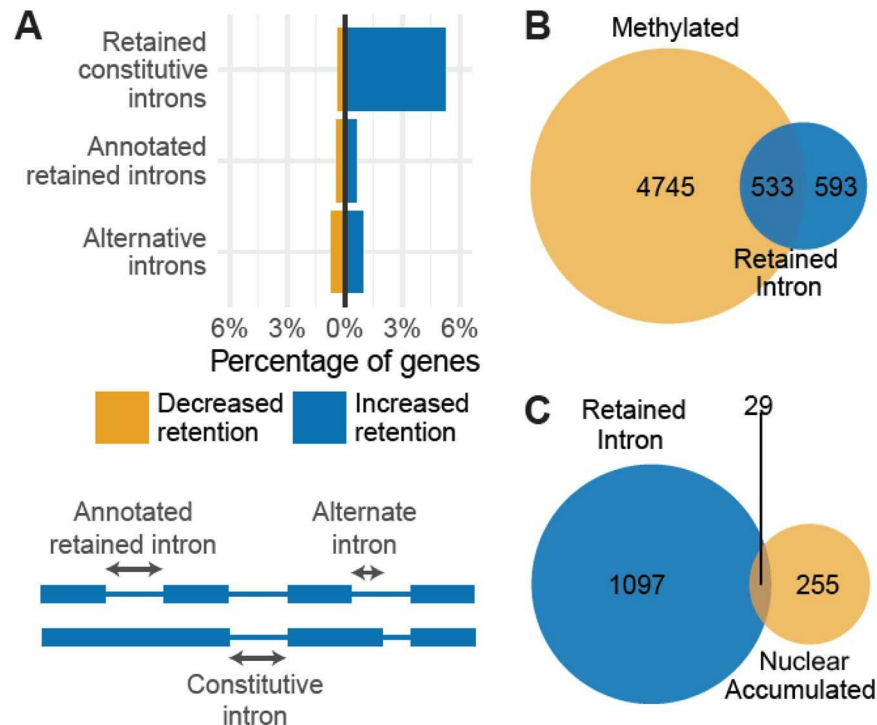


Figure 4. Effect of WTAP/KIAA1429 knockdown on intron retention. **(A)** Introns were divided into three categories (lower panel) – intron that is already annotated as being retained (Annotated retained intron), sequence that is always intronic in the annotation (Constitutive intron) and sequence that is sometimes intronic, sometimes exonic (Alternative intron). We measured the number of gene products containing an intron with evidence of a significant increase in intron retention (adjusted p -value < 0.1 ; $\log_{2}FC > 1$) for each intron type as a fraction of gene products that contained introns of that type (upper panel). **(B)** Overlap of gene products showed to be methylated (m^6A) with gene products showing evidence of increased intron retention on WTAP/KIAA1429 knockdown. **(C)** Overlap of gene products that show significant evidence of increased intron retention with gene products that show significant nuclear accumulation upon WTAP/KIAA1429 knockdown.

We also examined the overlap between gene products which had an mRNA export block and those which had retained introns and found that only 29 gene products with an mRNA export block had altered splicing (Fig. 4C; these 29 did not include DICER1 or PTPN12). 255 genes products had no detectable splicing defect and yet had a clear mRNA export block indicating that for the majority of mRNAs, the effect on mRNA export cannot be trivially explained by a defect in splicing.

YTHDC1 cooperates with TREX in mRNA export. Recent work has shown that knockdown of the methylation reader, YTHDC1, leads to nuclear retention of YTHDC1 target transcripts²⁸. We therefore investigated whether WTAP/KIAA1429 and YTHDC1 were acting in a common export pathway. We found that export targets for WTAP/KIAA1429 (Fig. 3A) are more downregulated on YTHDC1 knockdown than non-targets and the effects were similar in both cytoplasmic and nuclear RNA (Fig. S4). These data suggest that WTAP/KIAA1429 and YTHDC1 act on a common set of transcripts in mRNA export. To explore this further, we established a stable inducible YTHDC1 RNAi cell line and initially found that YTHDC1 was essential for cellular proliferation (Fig. S5B,C). We analysed the nuclear/cytoplasmic ratio following YTHDC1 RNAi and observed that TAF7, DICER1 and PTPN12, which were dependent on WTAP/KIAA1429 for mRNA export, had a dramatically increased nuclear/cytoplasmic ratio following YTHDC1 RNAi (Fig. 5A).

We noted that a recent large scale unbiased Co-IP mass spectrometry experiment analysed NXF2 as one of many baits and identified YTHDC1 as an interacting partner³⁷. NXF2 has a highly restricted expression pattern and is mainly expressed in testis. Therefore, we explored whether YTHDC1 might also interact with the more prevalent and sequence related mRNA export receptor, NXF1. These experiments revealed that YTHDC1 Co-IPed with ALYREF, DDX39B and CHTOP TREX subunits together with NXF1 (Fig. 5B,C). Although YTHDC1 was present in an NXF1 IP, we could not detect NXF1 in a YTHDC1 IP using an antibody to the endogenous protein, as reported by others²⁸, (data not shown), suggesting the YTHDC1 antibody might mask the region used to interact with NXF1 and TREX. Consistent with this explanation, the YTHDC1 antibody failed to immunoprecipitate any TREX subunits, in contrast to an ALYREF IP which pulled down TREX components and YTHDC1 (Fig. S5A). We conclude that TREX and NXF1 associate with YTHDC1 *in vivo*.

We further examined whether TREX might bridge the interaction between the methylase complex and YTHDC1 by immunoprecipitating WTAP in conditions where ALYREF and CHTOP were knocked down by RNAi (Fig. 5D). We found that YTHDC1 associated with WTAP and this interaction was insensitive to

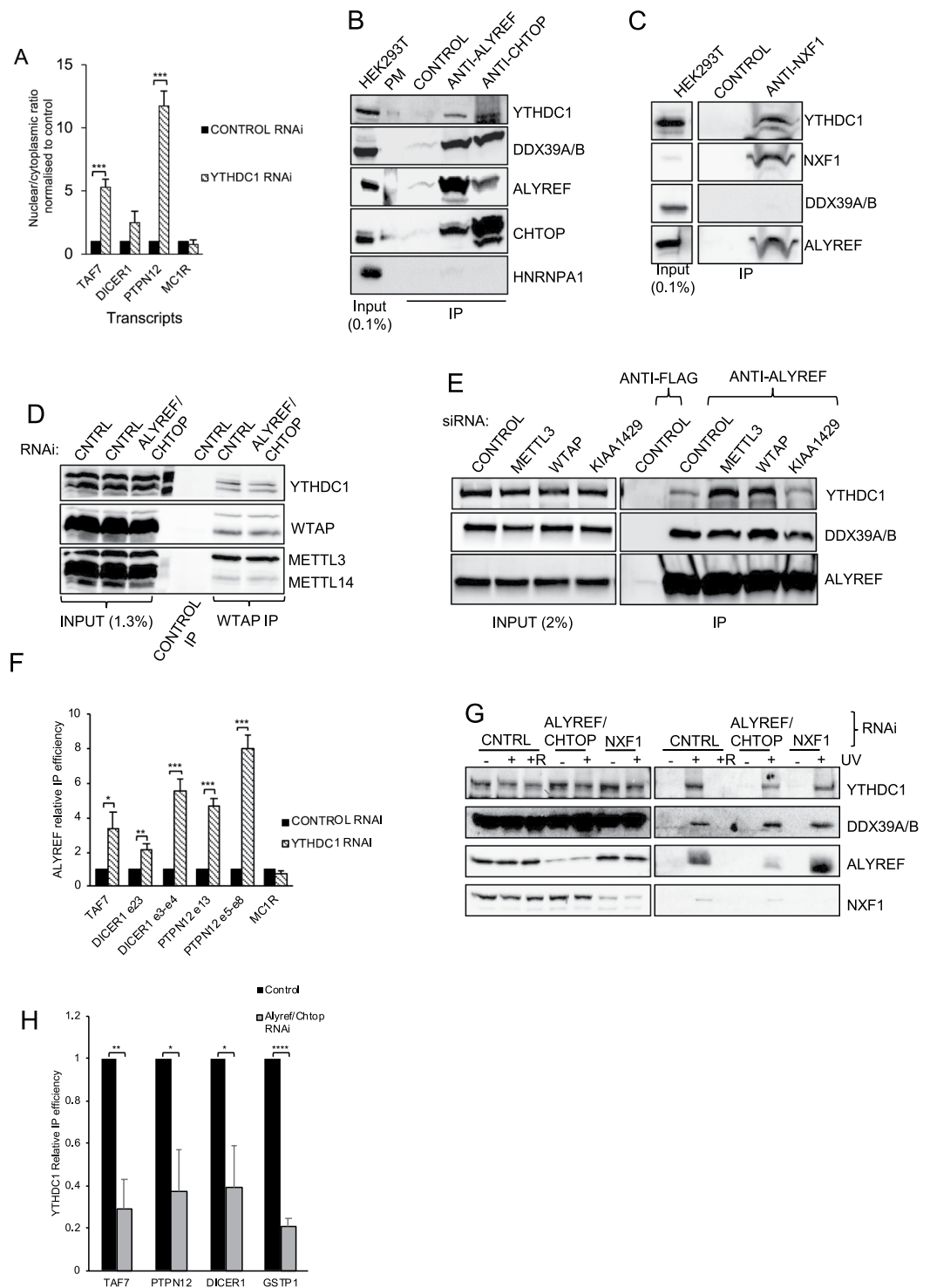


Figure 5. YTHDC1 associates with TREX and is required for mRNA export. **(A)** RT-qPCR analysis of the nuclear:cytoplasmic ratios for m⁶A modified (TAF7, DICER1, PTPN12) and non-modified (MC1R) transcripts following knockdown of YTHDC1. **(B)** Co-IP/Western analysis of ALYREF and CHTOP TREX subunits with YTHDC1 and other TREX subunits. PM = A lane where a protein marker was loaded. **(C)** Co-IP/Western analysis of NXF1 and YTHDC1. **(D)** WTAP co-IP/Western analysis with the indicated proteins in Control and ALYREF/CHTOP RNAi backgrounds **(E)** CO-IP/Western analysis of ALYREF with YTHDC1 and UAP56 in a background where METTL3, WTAP and KIAA1429 were knocked down using RNAi as indicated. **(F)** RT-qPCR RIP analysis of ALYREF in control RNAi and YTHDC1 RNAi cells. **(G)** UV crosslinking-mRNP capture analysis for the indicated proteins following depletion of ALYREF/CHTOP combined or NXF1. “R” indicates treatment with RNase A prior to oligo (dT) capture, as a control. **(H)** RT-qPCR RIP analysis of YTHDC1 in control and ALYREF/CHTOP RNAi cells. Where separate panels are shown for same the protein in Western blots, these are all taken from the same blot at the same exposure. Full size blots are displayed in Supplementary Information.

ALYREF/CHTOP levels. However, by immunoprecipitating ALYREF following depletion of METTL3, WTAP or KIAA1429 by RNAi (Fig. 5E), we discovered that reduced levels of either METTL3 or WTAP led to an increased association of YTHDC1 with ALYREF. These data suggest that whilst YTHDC1 and WTAP interact independently of TREX, WTAP and METTL3 regulate the association of TREX with YTHDC1. Therefore the m⁶A complex, TREX and YTHDC1 are functionally linked.

YTHDC1 recognises the m⁶A mark and may act downstream of the methylase complex. Therefore, we investigated what impact YTHDC1 depletion might have on the association of TREX with mRNA using an ALYREF RIP assay (Fig. 5F). Consistent with YTHDC1 acting downstream of ALYREF in mRNA export, we observed a significant increase in the amounts of mRNAs subject to m⁶A modification associated with ALYREF following knockdown of YTHDC1, rather than a decrease. One possible cause for increased association of ALYREF with mRNAs may be a failure to trigger the handover of mRNA to NXF1 by ALYREF which normally occurs during mRNA export³⁸. Since TREX associates with the methylase complex, we also investigated whether TREX was required for efficient association of YTHDC1 with poly(A)⁺ RNAs *in vivo* (Fig. 5G). Strikingly, we found that disruption of TREX following RNAi of the two key subunits ALYREF and CHTOP, reduced the association of YTHDC1 and NXF1 with poly(A)⁺ RNAs, yet DDX39A/B association, which lies upstream of TREX in the mRNA export complex assembly pathway¹, was unaltered. Using RIP assays we further established that knockdown of the TREX subunits ALYREF/CHTOP significantly reduced the association of YTHDC1 with selected mRNAs (Fig. 5H). Intriguingly, this effect was observed with both reported methylated transcripts (TAF7, PTPN12, DICER1) and the GSTP1 transcript which was not reported to be methylated. Further analysis of previously published YTHDC1 PAR-CLIP data²⁷, revealed that of the 1123 genes reproducibly found to be YTHDC1 targets in this study, only 39% were amongst the genes reported as methylated in either of the datasets we used. This suggests either the methylation data has a very low sensitivity or that YTHDC1 is able to bind mRNAs via an additional m⁶A-independent mechanism. Since we observed no export block for GSTP1 following WTAP/KIAA1429 RNAi (Fig. 2A) this would favour the latter explanation that YTHDC1 has a broader role in mRNA metabolism which goes beyond m⁶A control. Together these data suggest a model in which the m⁶A methylase complex recruits TREX to certain mRNAs and TREX additionally stimulates the recruitment of YTHDC1 and NXF1 triggering efficient mRNA export.

Discussion

In this study we have demonstrated an essential role for the m⁶A methylation complex in the recruitment of TREX to mRNAs modified by this complex and a further role for TREX in recruitment of YTHDC1 to mRNA. This provides a mechanistic explanation for the earlier observation that m⁶A methylation alters mRNA export kinetics²⁹. TREX subunits associate with m⁶A writer proteins, therefore the consensus sequence bound by the writer complex may be as important as the m⁶A modification itself, recruiting the writer complex to specific sites, together with RBM15/15B and TREX. The m⁶A writers thus drive early events associated with the mRNP such as TREX recruitment. TREX is further required for the efficient association of the m⁶A reader YTHDC1 with mRNAs and therefore TREX plays multiple roles in the mRNP interactions and exchanges which occur on mRNAs.

Why mRNAs which are subject to the m⁶A modification are dependent on the presence of the m⁶A methylase complex for recruitment of TREX whilst seemingly similar mRNAs without the m⁶A mark recruit TREX and get exported efficiently, is not clear. It may be the case that this modification allows recruitment of TREX to sites on mRNA which would otherwise be devoid of TREX. ALYREF is found along the entire body of mRNAs³⁹ and it associates with the exon junction complex (EJC) protein eIF4A3 which has a preferential binding site ~24 bases upstream from exon-exon junctions^{40,41}. Therefore, long internal exons and 3' UTRs which are enriched in m⁶A sites, may naturally be devoid of TREX recruitment options due to reduced levels of EJCs in the vicinity. Therefore, the m⁶A writer complex may act as a surrogate recruitment mechanism for TREX in these regions and facilitate subsequent recruitment of NXF1 to ensure efficient translocation of the mRNP through the nuclear pore. Consistent with this notion, we found that the m⁶A modified transcripts which showed nuclear accumulation following loss of the m⁶A writer complex had longer final exons on average (Fig. 3D).

An additional intriguing observation is that depletion of the methylase complex, triggers loss of TREX at multiple sites along an mRNA (Fig. 2D). This may be because m⁶A sites are under reported with existing technologies. Alternatively, TREX deposition at a single site may encourage stable binding of TREX at other sites along the mRNP, or it could be a combination of these effects. The EJC has been reported to form self-interactions and is proposed to aid with packaging of the mRNP⁴². Similarly, ALYREF is reported to interact with itself⁴³ and may help drive assembly of a compact mRNP with TREX-mRNP interactions stabilised by TREX-TREX interactions.

YTHDC1 was recently proposed to work in conjunction with SRSF3 in mRNA export and function in a complex with NXF1²⁸. We now show that TREX is an essential component for export of m⁶A modified mRNAs. When TREX associates with NXF1 it induces a conformational change such that it increases the RNA binding affinity up to ten fold³. However, this is a two component effect with ALYREF and SR proteins in isolation only able to increase the RNA binding activity of NXF1 approximately four fold³⁸. The additional RNA binding affinity associated with TREX recruitment comes from co-adaptor proteins within TREX such as THOC5 and CHTOP which associate with the NTF2L domain of NXF1. This disrupts the sequestration of the N-terminal NXF1 RNA binding domain^{3,4} leading to maximal RNA binding activity and stable association of NXF1 with the mRNP. Therefore, it is highly likely that SR proteins work in conjunction with co-adaptor proteins or even a complete TREX complex to facilitate NXF1 recruitment to m⁶A modified and non-modified mRNAs. Consistent with this, yeast SR proteins are known to associate with TREX⁴⁴. In summary, we have identified an essential function for the m⁶A methylation machinery in mRNA export and demonstrated that this function is mediated through TREX.

Methods

siRNA transfections. siRNA transfections of 60% confluent 293 T cells grown in Dulbecco's Modified Eagles Medium were carried out using RNAiMAX (Life technologies) with siRNAs at 10 nM. Silencer select siRNA ID S24832 Cat No. 4392420 targeting KIAA1429 was purchased from ThermoFisher Scientific. The siRNA targeting WTAP was described previously¹⁶ and had the following sequence: 5'-GGCAAGAGAUGAGUUAUUCUAAGA. For METTL3, Stealth siRNA HSI125548 from ThermoFischer Scientific was used. The control siRNA was described previously⁴⁵. siRNA transfected cells were incubated for 72 hours undergoing a second transfection at 48 hours. YTHDC1 RNAi was carried out using a stably integrated miR30 mimic RNAi cassette in Flp-In HEK293 cells as described previously³⁴. The cassette contained two hairpins targeting the following sequences 5' GAGAATGTGTCTCTTGCCAAA and 5' CAGAGATAAACGAGTACATGA. The NXF1, ALYREF/CHTOP and Control inducible RNAi cell lines have been described previously^{3,4}. Growth of YTHDC1 RNAi cells was assessed using an MTT assay⁴⁶.

Fluorescence In-Site Hybridisation (FISH). FISH was carried out as described previously³⁸.

Co-IPs. Each sample used 100 µl Protein-G DYNA beads blocked over night at 4 °C in 500 µl of IP lysis buffer (50 mM HEPES-NaOH pH 7.5, 100 mM NaCl, 1 mM EDTA pH 8.0, 0.1% Triton X-100, 10% Glycerol, 1 mM DTT) containing 1% BSA and 2–10 µg of antibody. Beads were subsequently washed 3 times in 1 ml IP lysis buffer. Cells were washed with PBS before lysis in IP lysis buffer containing protease inhibitor, DNase 1, RNase A and DTT. Extracts were cleared by centrifugation at 13 200 rpm, 5 minutes at 4 °C. Cell extracts were incubated with antibody bound beads for 2 hours at 4 °C. Beads were washed 3 times in 1 ml ice cold IP lysis buffer. After the final wash beads were resuspend in 72 µl 1 M Arginine-HCl pH 3.5, incubated for 1 minute on ice and spun for 1 minute at 400 × g. Eluate was transferred to a fresh 1.5 ml tube and neutralised with 3 µl 1.5 M Tris.HCl (pH 8.8) prior to SDS-PAGE. Antibodies used in this study were: FLAG – Sigma F3165, WTAP Santa Cruz sc-374280 (used for Fig. 1A), WTAP Abcam Ab195380 used for remaining Figures, KIAA1429 – Proteintech 25712-1-AP, METTL3 – Proteintech 15073-1-AP, HNRNPA1 – Millipore 04-1469, METTL14 – Sigma HPA038002, ACTIN – Sigma A5060, YTHDC1 – Proteintech 14392-1-AP, SSRP1 – Biologend 609701, TUBULIN – Sigma T5168, ALYREF – Abcam Ab6141, NXF1 – Abcam Ab50609, DDX39A/B and THOC5 were described previously³.

RNA/Protein extraction from 293 T cells. 2 × 10 cm dishes were used and nuclear/cytoplasmic fractionations were performed as described previously⁴⁷. Nuclei obtained with this procedure were fractionated into nucleoplasm and chromatin as described previously⁴⁸. The RNA content from each fraction was extracted using TRIzol. RNA samples were DNase-treated (TurboDNase, Ambion). Fractionations were assessed by western blot analysis, using histone H3, as a chromatin marker, SSRP1 as nuclear marker, and TUBULIN as a cytoplasmic marker.

Formaldehyde RNA Immuno-Precipitation (faRIP). One 6-cm dish (or 2 × 6-cm dishes for siRNA treatments) was seeded per RIP condition with 3 × 10⁵ cells/dish. Protein-RNA complexes were crosslinked *in vivo* by incubating cells with 3 mL of PBS-Formaldehyde (0.1%), as described previously⁴⁹. 100 µl of protein G-Dynabeads® beads were prepared by initial washing with 3 × 1 mL RIP lysis buffer (50 mM HEPES-HCl pH 7.5, 150 mM NaCl, 10% glycerol 1% NP-40, 0.1% SDS, and 0.5% sodium deoxycholate) before being blocked and loaded with the relevant antibody (2–10 µg diluted in 0.3 mL of RIP lysis buffer +1% BSA w/v final) for 1 hour at room temperature. Beads were washed with 3 × 1 mL RIP lysis buffer and left on ice. Each cell pellet was lysed in 400 µl RIP lysis buffer supplemented with 1 mM DTT, protease inhibitors (SigmaFAST, Sigma), 2 µl of RNase inhibitors (Ribosafe, Bionline) and 2 µl/mL of Turbo DNase (Ambion). Samples were sonicated using a Bioruptor (High, 5 × [30s-ON/30s-OFF]) and cleared by centrifugation (16100 × g, 10 min, 4 °C). 300 µl of each sample was incubated with Dynabeads for 2 hours at 4 °C and 30 µl of lysate was kept as input (10%). Following incubation, the beads were washed with 2 × 1 mL RIP lysis buffer, 2 × 1 mL high salt RIP lysis buffer (adjusted to 500 mM NaCl, 5 min each on ice), and 2 × 1 mL RIP lysis buffer. Elutions were performed as described previously⁴⁹. The RNA content of the resulting eluates and inputs were extracted using TRIzol. RNA samples were DNase-treated (Turbo DNase, Ambion) and used for cDNA synthesis and RT-qPCR analysis. Oligonucleotides used for RT-qPCR analysis were as follows: TAF7 Forward 5' GCCTCTACTGTGAGAAGGGG, TAF7 Reverse 5' CACGGTCCACTCTGACGATT, DICER1 e23 Forward 5' CATAGCGGACTGTGTGTGGAAG, DICER1 e23 Reverse 5' AGCAGCACAGCTCACTGAAA, DICER1 e3 Forward 5' GACTTGCTATGTCGCCTTGA, DICER1 e4 Reverse 5' ATGCGAGGACATGATGGA, PTPN12 e13 Forward 5' ACTCTGATGGTGTGTGACC, PTPN12 e13 Reverse 5' GCACCTGAATGTGTGTGTTCC, PTPN12 e5 Forward 5' GAGCGCTATTGGCCTTTG, PTPN12 e8 Reverse 5' AATGGCACCTGTCTTCCAC, GSTP1 Forward 5' CCGTGGTCTATTTCCAGTT, GSTP1 Reverse 5' AGGTGACGCAGGATGGTATT, SYMPK Forward 5' AACCAGACCAGAAGGATGG, SYMPK Reverse 5' AGTACTTGCGGACCACCTC, MC1R Forward 5' GGACCGTACATCCCATCT, MC1R Reverse 5' GCATAGCCAGGAAGAAGACC, U1 Forward 5' ACCTGGCAGGGGAGATACC, U1 Reverse 5' GGGGAAAGCGCGAACGCAGT. IP efficiencies were calculated relative to the input RNA levels.

mRNP capture assays. 1 × 15 cm dish of cells was used per condition. 2 × binding buffer (BB) (20 mM HEPES-K-NaOH pH 7.5, 1 M NaCl, 1% SDS, 0.2 mM EDTA pH 8) was preheated to 37 °C. 1 × binding buffer was made by mixing 1:1 mRNP lysis buffer (LB) (50 mM HEPES-K-NaOH pH 7.5, 100 mM NaCl, 1 mM DTT, 1 mM EDTA pH 8.0, 0.5% Igepal Ca-630/NP-40, 0.5% Na-deoxycholate, 10% glycerol) with preheated 2 × BB. 100 µl of magnetic oligo dT beads (New England Biolabs) were used per sample and washed 3 times in 1 × BB. Cells were crosslinked with 300 mJ/cm² ultraviolet light (UV). Each dish of cells was lysed in 600 µl LB supplemented with protease inhibitor cocktail and RNase inhibitors. Post lysis, samples were spun at 4 °C, 16100 g for 10 minutes. Samples were denatured by adding 1:1 lysate and 2 × BB at 37 °C. Denatured lysates were added to the beads and

incubated for 1 hour at 25 °C. Samples were washed 3 times in 1 x BB and eluted in 60 µl of mRNP elution buffer (10 mM Tris pH 7.5, 1 mM EDTA pH 8) supplemented with RNase A (50 µg/mL⁻¹). Elution was carried out at 25 °C shaking at 800 rpm for 30 minutes.

mRNA Sequencing. Libraries for sequencing were prepared using the Lexogen SENSE mRNA-Seq Library Prep according to the manufacturer's instructions and sequenced using a HiSeq2500.

Computational Analysis. Read Preprocessing. Nine nucleotides were removed from read 1 fastq files, and six were removed from read 2, as suggested by the Lexogen SENSE library preparation manual using the cutadapt tool⁵⁰. Samples split across two lanes were merged into a single fastq file. Transcript Abundance Quantification. Transcript abundances were estimated using salmon⁵¹ against the Ensembl v75 annotation (as the hg19 genome was used for the m6A iCLIP data)⁵². Abundances were then aggregated to gene level using tximport⁵³. Differential Nuclear Retention Analysis. Differential nuclear retention of genes was calculated using edgeR⁵⁴, using the contrast formula: $(KD_{nuc}/KD_{cyt})/(WT_{nuc}/WT_{cyt})$. Genes with a log fold change greater than 0.5 and an FDR less than 0.1 were considered significantly accumulating in the nucleus, and used for downstream analyses. Overlap with m⁶A iCLIP data: RNA methylation sites were obtained as bed files from an m⁶A iCLIP (miCLIP) dataset⁵². The number of miCLIP sites overlapping exonic regions of each gene was counted using bedtools intersect⁵⁵. Any gene that contained at least one overlapping miCLIP site from either m6A antibody was considered to be methylated. P-values for the intersection of methylated genes with nuclear accumulating genes were calculated using hypergeometric tests. Intron Retention Analysis: Reads were mapped to hg19 using HiSat⁵⁶ with default parameters. Gene models were obtained from Ensembl v75 and divided into minimally spanning transcript chunks using the gtf2gtf program from the CGAT suite⁵⁷ and annotated as either constitutive exon, constitutive intron, annotated retained intron or alternate (see code). Read counts were calculated using featureCounts from the subread package⁵⁸ and differential chunk usage calculated using DEXSeq⁵⁹. Intron chunks with and adjust p-value less than 0.1 and a log₂ fold change between control and WTAP/KIAA1429 > 1 were designated as significantly more retained. Further Analysis: Final exon length distributions were calculated using custom python scripts which are available from Zenodo, <https://doi.org/10.5281/zenodo.1194638>.

Data Availability

The RNA-seq data have been submitted to GEO Accession Number: GSE111878.

References

- Heath, C. G., Viphacone, N. & Wilson, S. A. The role of TREX in gene expression and disease. *Biochem J* **473**, 2911–2935 (2016).
- Fan, J. *et al.* Exosome cofactor hMTR4 competes with export adaptor ALYREF to ensure balanced nuclear RNA pools for degradation and export. *Embo J* **36**, 2870–2886 (2017).
- Viphacone, N. *et al.* TREX exposes the RNA-binding domain of Nxf1 to enable mRNA export. *Nat Commun* **3**, 1006 (2012).
- Chang, C. T. *et al.* Chtop is a component of the dynamic TREX mRNA export complex. *Embo J* **32**, 473–486 (2013).
- Huang, Y., Gattoni, R., Stevenin, J. & Steitz, J. A. SR splicing factors serve as adapter proteins for TAP-dependent mRNA export. *Mol. Cell* **11**, 837–843 (2003).
- Hargous, Y. *et al.* Molecular basis of RNA recognition and TAP binding by the SR proteins SRp20 and 9G8. *Embo J* **25**, 5126–5137 (2006).
- Desrosiers, R., Friderici, K. & Rottman, F. Identification of methylated nucleosides in messenger RNA from Novikoff hepatoma cells. *Proc Natl Acad Sci USA* **71**, 3971–3975 (1974).
- Ke, S. *et al.* m(6A) mRNA modifications are deposited in nascent pre-mRNA and are not required for splicing but do specify cytoplasmic turnover. *Genes Dev* **31**, 990–1006 (2017).
- Zhao, B. S., Roundtree, I. A. & He, C. Post-transcriptional gene regulation by mRNA modifications. *Nat Rev Mol Cell Biol* **18**, 31–42 (2016).
- Hausmann, I. U. *et al.* m(6A) potentiates Sxl alternative pre-mRNA splicing for robust Drosophila sex determination. *Nature* **540**, 301–304 (2016).
- Domisissini, D. *et al.* Topology of the human and mouse m6A RNA methylomes revealed by m6A-seq. *Nature* **485**, 201–206 (2012).
- Meyer, K. D. *et al.* Comprehensive analysis of mRNA methylation reveals enrichment in 3' UTRs and near stop codons. *Cell* **149**, 1635–1646 (2012).
- Ke, S. *et al.* A majority of m6A residues are in the last exons, allowing the potential for 3' UTR regulation. *Genes Dev* **29**, 2037–2053 (2015).
- Liu, J. *et al.* A METTL3-METTL14 complex mediates mammalian nuclear RNA N6-adenosine methylation. *Nat Chem Biol* **10**, 93–95 (2014).
- Schwartz, S. *et al.* Perturbation of m6A writers reveals two distinct classes of mRNA methylation at internal and 5' sites. *Cell Rep* **8**, 284–296 (2014).
- Patil, D. P. *et al.* m(6A) RNA methylation promotes XIST-mediated transcriptional repression. *Nature* **537**, 369–373 (2016).
- Zolotukhin, A. S. *et al.* Nuclear export factor RBM15 facilitates the access of DBP5 to mRNA. *Nucleic Acids Res* **37**, 7151–7162 (2009).
- Uranishi, H. *et al.* The RNA-binding motif protein 15B (RBM15B/OTT3) acts as cofactor of the nuclear export receptor NXF1. *J Biol Chem* **284**, 26106–26116 (2009).
- Knuckles, P. *et al.* Zc3h13/Flacc is required for adenosine methylation by bridging the mRNA-binding factor Rbm15/Spenito to the m(6A) machinery component Wtap/FI(2)d. *Genes Dev* **32**, 415–429 (2018).
- Wen, J. *et al.* Zc3h13 Regulates Nuclear RNA m(6A) Methylation and Mouse Embryonic Stem Cell Self-Renewal. *Mol Cell* **69**, 1028–1038 e1026 (2018).
- Li, F., Zhao, D., Wu, J. & Shi, Y. Structure of the YTH domain of human YTHDF2 in complex with an m(6A) mononucleotide reveals an aromatic cage for m(6A) recognition. *Cell research* **24**, 1490–1492 (2014).
- Xu, C. *et al.* Structural Basis for the Discriminative Recognition of N6-Methyladenosine RNA by the Human YT521-B Homology Domain Family of Proteins. *J Biol Chem* **290**, 24902–24913 (2015).
- Xu, C. *et al.* Structural basis for selective binding of m6A RNA by the YTHDC1 YTH domain. *Nat Chem Biol* **10**, 927–929 (2014).
- Alarcon, C. R. *et al.* HNRNPA2B1 Is a Mediator of m(6A)-Dependent Nuclear RNA Processing Events. *Cell* **162**, 1299–1308 (2015).
- Liu, N. *et al.* N(6)-methyladenosine-dependent RNA structural switches regulate RNA-protein interactions. *Nature* **518**, 560–564 (2015).

26. Du, H. *et al.* YTHDF2 destabilizes m(6)A-containing RNA through direct recruitment of the CCR4-NOT deadenylase complex. *Nat Commun* **7**, 12626 (2016).
27. Xiao, W. *et al.* Nuclear m(6)A Reader YTHDC1 Regulates mRNA Splicing. *Mol Cell* **61**, 507–519 (2016).
28. Roundtree, I. A. *et al.* YTHDC1 mediates nuclear export of N(6)-methyladenosine methylated mRNAs. *eLife* **6** (2017).
29. Fustin, J. M. *et al.* RNA-methylation-dependent RNA processing controls the speed of the circadian clock. *Cell* **155**, 793–806 (2013).
30. Mauer, J. *et al.* Reversible methylation of m(6)Am in the 5' cap controls mRNA stability. *Nature* **541**, 371–375 (2017).
31. Zheng, G. *et al.* ALKBH5 is a mammalian RNA demethylase that impacts RNA metabolism and mouse fertility. *Mol Cell* **49**, 18–29 (2013).
32. Horiuchi, K. *et al.* Identification of Wilms' tumor 1-associating protein complex and its role in alternative splicing and the cell cycle. *J Biol Chem* **288**, 33292–33302 (2013).
33. Ping, X. L. *et al.* Mammalian WTAP is a regulatory subunit of the RNA N6-methyladenosine methyltransferase. *Cell research* **24**, 177–189 (2014).
34. Hautbergue, G. M. *et al.* UIF, a New mRNA Export Adaptor Which Works Together with REF/ALY, Requires FACT for Recruitment to mRNA. *Curr Biol* **19**, 1918–1924 (2009).
35. Palazzo, A. F. *et al.* The signal sequence coding region promotes nuclear export of mRNA. *PLoS biology* **5**, e322 (2007).
36. Ortega, A. *et al.* Biochemical function of female-lethal (2)D/Wilms' tumor suppressor-1-associated proteins in alternative pre-mRNA splicing. *J Biol Chem* **278**, 3040–3047 (2003).
37. Huttlin, E. L. *et al.* Architecture of the human interactome defines protein communities and disease networks. *Nature* **545**, 505–509 (2017).
38. Hautbergue, G. M., Hung, M. L., Golovanov, A. P., Lian, L. Y. & Wilson, S. A. Mutually exclusive interactions drive handover of mRNA from export adaptors to TAP. *Proc Natl Acad Sci USA* **105**, 5154–5159 (2008).
39. Shi, M. *et al.* ALYREF mainly binds to the 5' and the 3' regions of the mRNA *in vivo*. *Nucleic Acids Res* **45**, 9640–9653 (2017).
40. Le Hir, H., Gatfield, D., Izaurralde, E. & Moore, M. J. The exon-exon junction complex provides a binding platform for factors involved in mRNA export and nonsense-mediated mRNA decay. *Embo J* **20**, 4987–4997 (2001).
41. Gromadzka, A. M., Steckelberg, A. L., Singh, K. K., Hofmann, K. & Gehring, N. H. A short conserved motif in ALYREF directs cap- and EJC-dependent assembly of export complexes on spliced mRNAs. *Nucleic Acids Res* **44**, 2348–2361 (2016).
42. Singh, G. *et al.* The cellular EJC interactome reveals higher-order mRNP structure and an EJC-SR protein nexus. *Cell* **151**, 750–764 (2012).
43. Rodrigues, J. P. *et al.* REF proteins mediate the export of spliced and unspliced mRNAs from the nucleus. *Proc Natl Acad Sci USA* **98**, 1030–1035 (2001).
44. Hurt, E., Luo, M. J., Rother, S., Reed, R. & Strasser, K. Cotranscriptional recruitment of the serine-arginine-rich (SR)-like proteins Gbp2 and Hrb1 to nascent mRNA via the TREX complex. *Proc Natl Acad Sci USA* **101**, 1858–1862 (2004).
45. Viphakone, N. *et al.* Luzzp4 defines a new mRNA export pathway in cancer cells. *Nucleic Acids Res* **43**, 2353–2366 (2015).
46. van de Loosdrecht, A. A., Beelen, R. H., Ossenkoppele, G. J., Broekhoven, M. G. & Langenhuijsen, M. M. A tetrazolium-based colorimetric MTT assay to quantitate human monocyte mediated cytotoxicity against leukemic cells from cell lines and patients with acute myeloid leukemia. *Journal of immunological methods* **174**, 311–320 (1994).
47. Stubbs, S. H. & Conrad, N. K. Depletion of REF/Aly alters gene expression and reduces RNA polymerase II occupancy. *Nucleic Acids Res* **43**, 504–519 (2015).
48. Werner, M. S. & Ruthenburg, A. J. Nuclear Fractionation Reveals Thousands of Chromatin-Tethered Noncoding RNAs Adjacent to Active Genes. *Cell Rep* **12**, 1089–1098 (2015).
49. David, G. H., Kelley, D. R., Tenen, D., Bernstein, B. & Rinn, J. L. Widespread RNA binding by chromatin-associated proteins. *Genome Biol* **17**, 28 (2016).
50. Martin, M. Cutadapt removes adapter sequences from high-throughput sequencing reads. *EMBnet.Journal* **17**, 10–12 (2011).
51. Patro, R., Duggal, G., Love, M. I., Irizarry, R. A. & Kingsford, C. Salmon provides fast and bias-aware quantification of transcript expression. *Nat Methods* **14**, 417–419 (2017).
52. Linder, B. *et al.* Single-nucleotide-resolution mapping of m6A and m6Am throughout the transcriptome. *Nat Methods* **12**, 767–772 (2015).
53. Soneson, C., Love, M. I. & Robinson, M. D. Differential analyses for RNA-seq: transcript-level estimates improve gene-level inferences. *F1000Res* **4**, 1521 (2015).
54. McCarthy, D. J., Chen, Y. & Smyth, G. K. Differential expression analysis of multifactor RNA-Seq experiments with respect to biological variation. *Nucleic Acids Res* **40**, 4288–4297 (2012).
55. Quinlan, A. R. & Hall, I. M. BEDTools: a flexible suite of utilities for comparing genomic features. *Bioinformatics* **26**, 841–842 (2010).
56. Kim, D., Langmead, B. & Salzberg, S. L. HISAT: a fast spliced aligner with low memory requirements. *Nat Methods* **12**, 357–360 (2015).
57. Sims, D. *et al.* CGAT: computational genomics analysis toolkit. *Bioinformatics* **30**, 1290–1291 (2014).
58. Liao, Y., Smyth, G. K. & Shi, W. featureCounts: an efficient general purpose program for assigning sequence reads to genomic features. *Bioinformatics* **30**, 923–930 (2014).
59. Anders, S., Reyes, A. & Huber, W. Detecting differential usage of exons from RNA-seq data. *Genome Res* **22**, 2008–2017 (2012).

Acknowledgements

We acknowledge support from the Biotechnology and Biological Sciences Research Council (BBSRC, UK) through grants BB/N014839/1 and BB/N005430/1. SL was supported by a BBSRC White Rose Doctoral Training Programme studentship.

Author Contributions

S.L., N.V. and C.H. carried out the laboratory experiments. M.P., J.P. and I.S. carried out the bioinformatic analyses. S.L., N.V. and S.W. designed the experiments and interpreted the results. S.W. conceived the study. S.L. and S.W. wrote the manuscript. All authors read and approved the final manuscript.

Additional Information

Supplementary information accompanies this paper at <https://doi.org/10.1038/s41598-018-32310-8>.

Competing Interests: The authors declare no competing interests.

Publisher's note: Springer Nature remains neutral with regard to jurisdictional claims in published maps and institutional affiliations.



Open Access This article is licensed under a Creative Commons Attribution 4.0 International License, which permits use, sharing, adaptation, distribution and reproduction in any medium or format, as long as you give appropriate credit to the original author(s) and the source, provide a link to the Creative Commons license, and indicate if changes were made. The images or other third party material in this article are included in the article's Creative Commons license, unless indicated otherwise in a credit line to the material. If material is not included in the article's Creative Commons license and your intended use is not permitted by statutory regulation or exceeds the permitted use, you will need to obtain permission directly from the copyright holder. To view a copy of this license, visit <http://creativecommons.org/licenses/by/4.0/>.

© The Author(s) 2018

Title: The m⁶A-methylase complex recruits TREX and regulates mRNA export.

Authors: Simon Lesbirel^a, Nicolas Viphakone^a, Matthew Parker^a, Jacob Parker^a, Catherine Heath^a, Ian Sudbery^a and Stuart A. Wilson^{a,*}

^aSheffield Institute For Nucleic Acids (SInFoNiA), Department of Molecular Biology and Biotechnology, University of Sheffield, Firth Court Western Bank, Sheffield, S10 2TN, U.K.

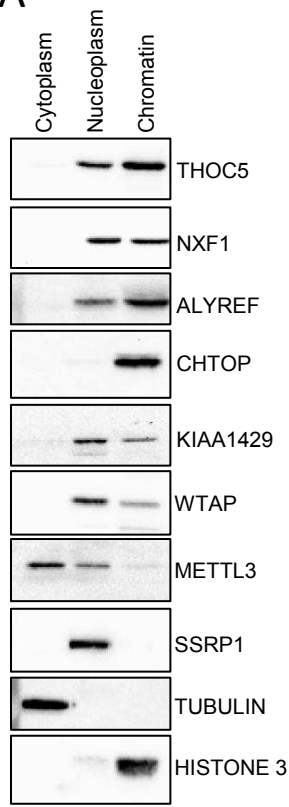
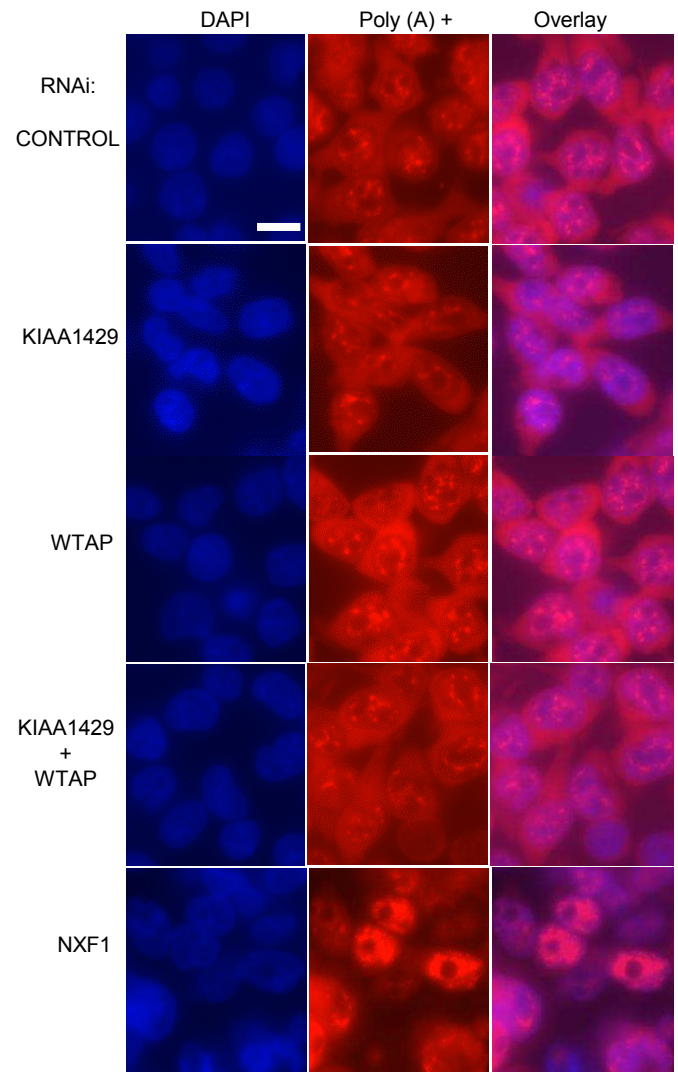
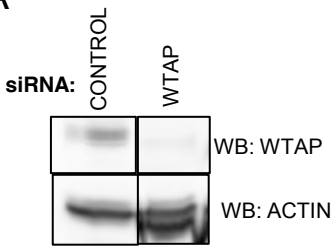
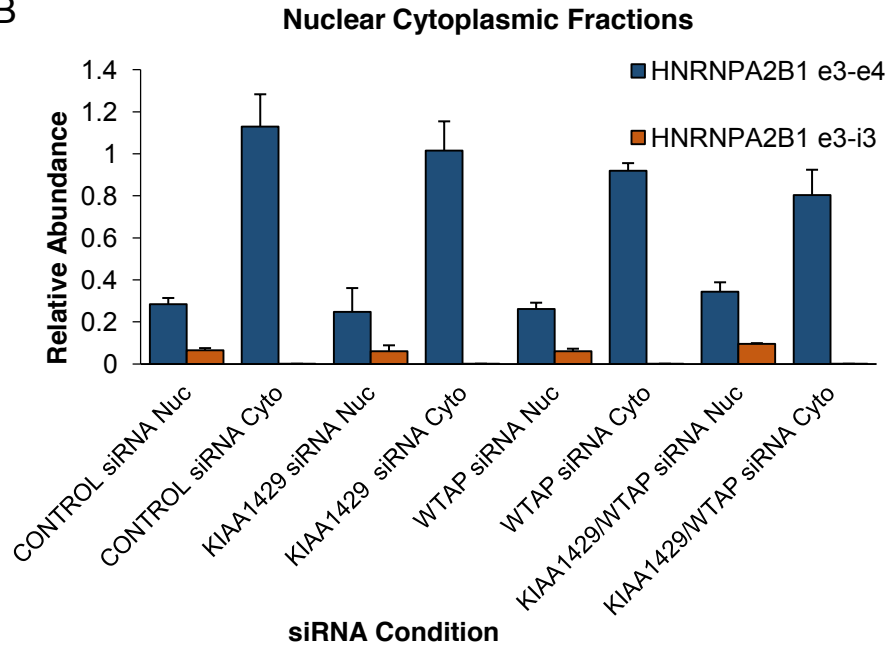
A**B**

Fig. S1. Analysis of KIAA1429 and WTAP in mRNA export. A) Western analysis of subcellular fractions for the indicated proteins. SSRP1, Histone H3 and Tubulin were used as markers for each of the three subcellular fractions. B) oligodT fluorescence *in situ* hybridisation analysis of cells following knockdown of the indicated genes by RNAi. For the NXF1 RNAi a stable cell line was used which expressed a miRNA targeting NXF1 as described previously³. The scale bar is 10µM.

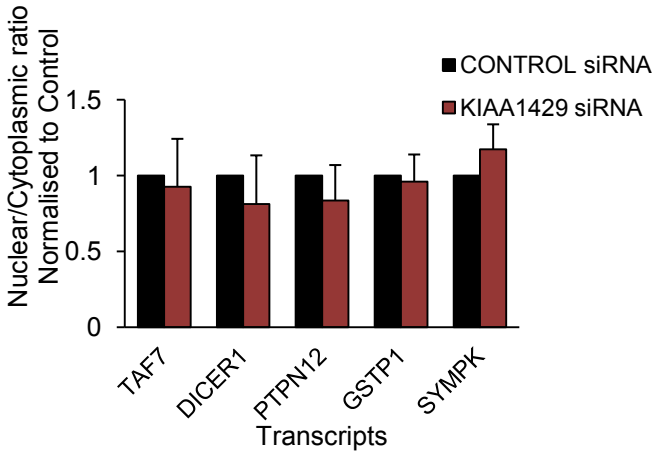
A



B



C



D

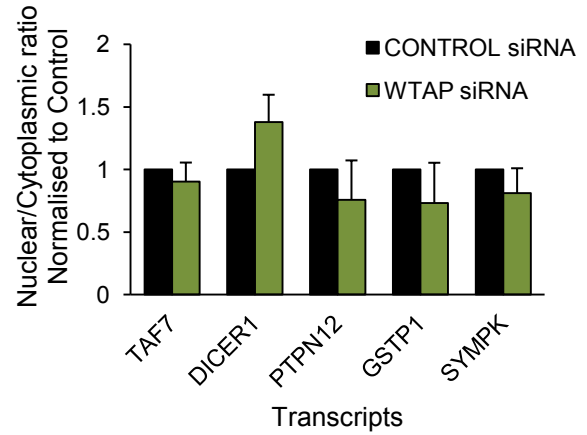


Fig. S2. mRNA Analysis of KIAA1429 and WTAP in mRNA export. A) Western analysis showing efficient knockdown of WTAP following transfection of cells with WTAP siRNA. B) qRT-PCR analysis showing efficient fractionation of subcellular compartments. The unspliced pre-mRNA is only detected in the nuclear fractions whereas the spliced mRNA is detected in both subcellular fractions. C,D) qRT-PCR analysis of nuclear/cytoplasmic ratios for selected transcripts (m⁶A modified: TAF7, PTPN12, DICER1; non-modified: GSTP1, SYMPK) following individual knockdown of either WTAP or KIAA1429. Where separate panels are shown for the same protein in Fig. S1A, the panels were taken from the same blot at the same exposure.

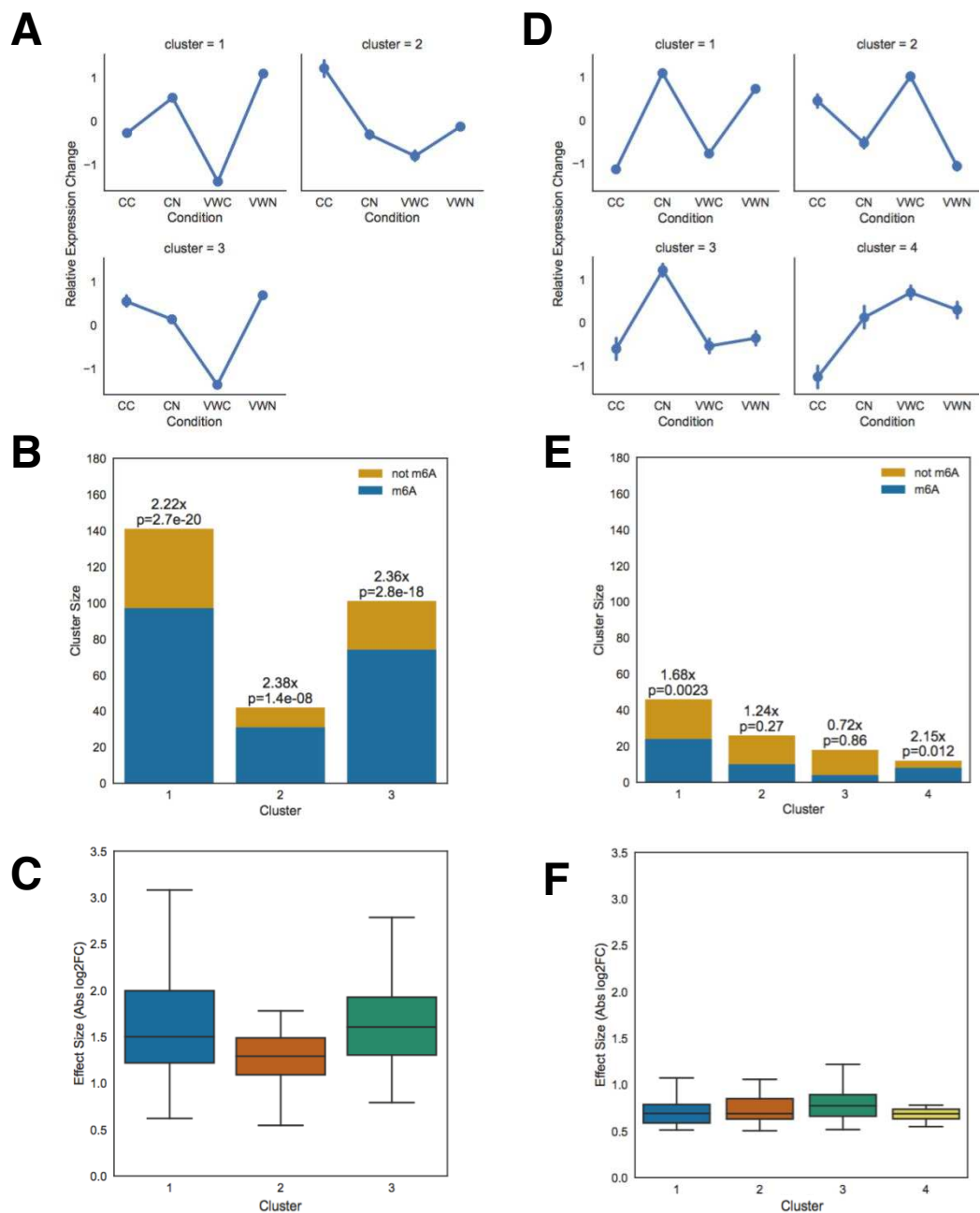
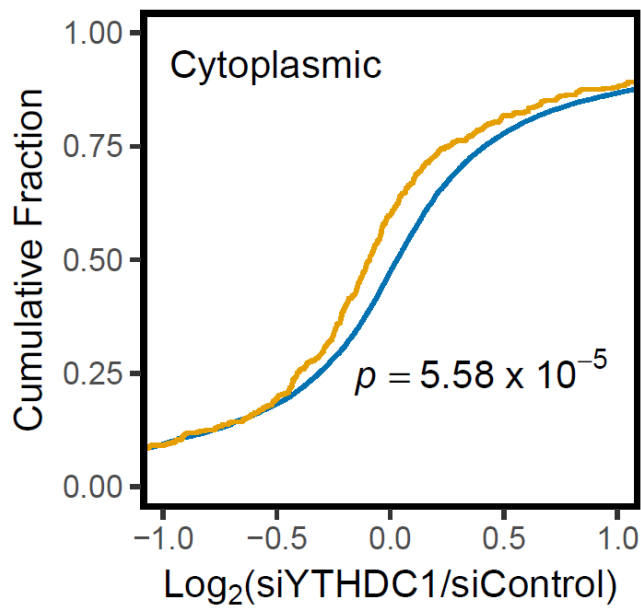
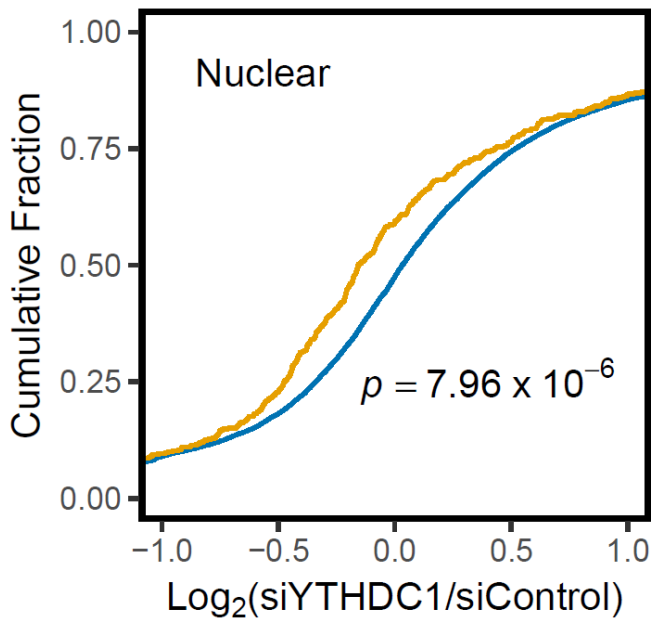


Fig. S3: Patterns of gene expression in differentially retained or exported genes. A) K-means clustering of nuclear accumulating genes suggests three clusters, showing two main patterns of gene expression. Clusters one and three contain genes with nuclear/cytoplasmic ratios greater than one and less than one, respectively, which show nuclear accumulation (increase in nuclear level and reduction in cytoplasmic level) during WTAP/KIAA1429 knockdown. Cluster two contains genes which exhibit reduction in cytoplasmic level with little or no increase in nuclear level. B) Cluster sizes for nuclear accumulating gene clusters. 86% of genes show a pattern of nuclear accumulation and cytoplasmic reduction, suggesting the majority of the effect is caused by an mRNA export block. All clusters show similarly high levels of methylation detection in the miCLIP dataset. Fold enrichment of methylation in clusters over all genes and hypogeometric p-value for enrichment are shown above the bars C) Distribution of changes in nuclear accumulation for each cluster. D, E and F) As A, B and C but for cytoplasmically accumulating genes. Clusters one and two: genes with nuclear/cytoplasmic ratios of greater than one and less than one, respectively and reduced nuclear levels and increased cytoplasmic levels following WTAP/KIAA1429 RNAi. Cluster three: genes with reduced nuclear expression and no significant change in cytoplasmic levels. Cluster four: genes which show an increase in cytoplasmic expression with no corresponding reduction in nuclear expression. 70% of genes show a pattern of cytoplasmic accumulation and nuclear reduction, suggesting the majority of the effect is caused by an increase in export. Throughout the Figure: CC = Control cytoplasmic fraction, CN = Control Nuclear Fraction, VWC = KIAA1429/WTAP RNAi cytoplasmic fraction, VWN = KIAA1429/WTAP RNAi nuclear fraction.



WTAP
Target Status — Non-Target — Target



WTAP
Target Status — Non-Target — Target

Fig. S4. WTAP/KIAA1429 targets are down-regulated on YTHDC1 knockdown. Plots show the cumulative distribution function of log-fold changes in transcript expression on YTHDC1 knockdown using data from (eLife 2017;6:e31311 DOI: [10.7554/ELIFE.31311](https://doi.org/10.7554/ELIFE.31311)). Log-fold change calculated as the average ratio of expression between knockdown and control for two different YTHDC1 siRNAs for both nuclear and cytoplasmic RNA fractions as indicated. Functions shown separately for nuclear retention targets of WTAP/KIAA1429 and non-targets. P-value for the difference between targets and non-targets calculated using the Mann-Whitney U test.

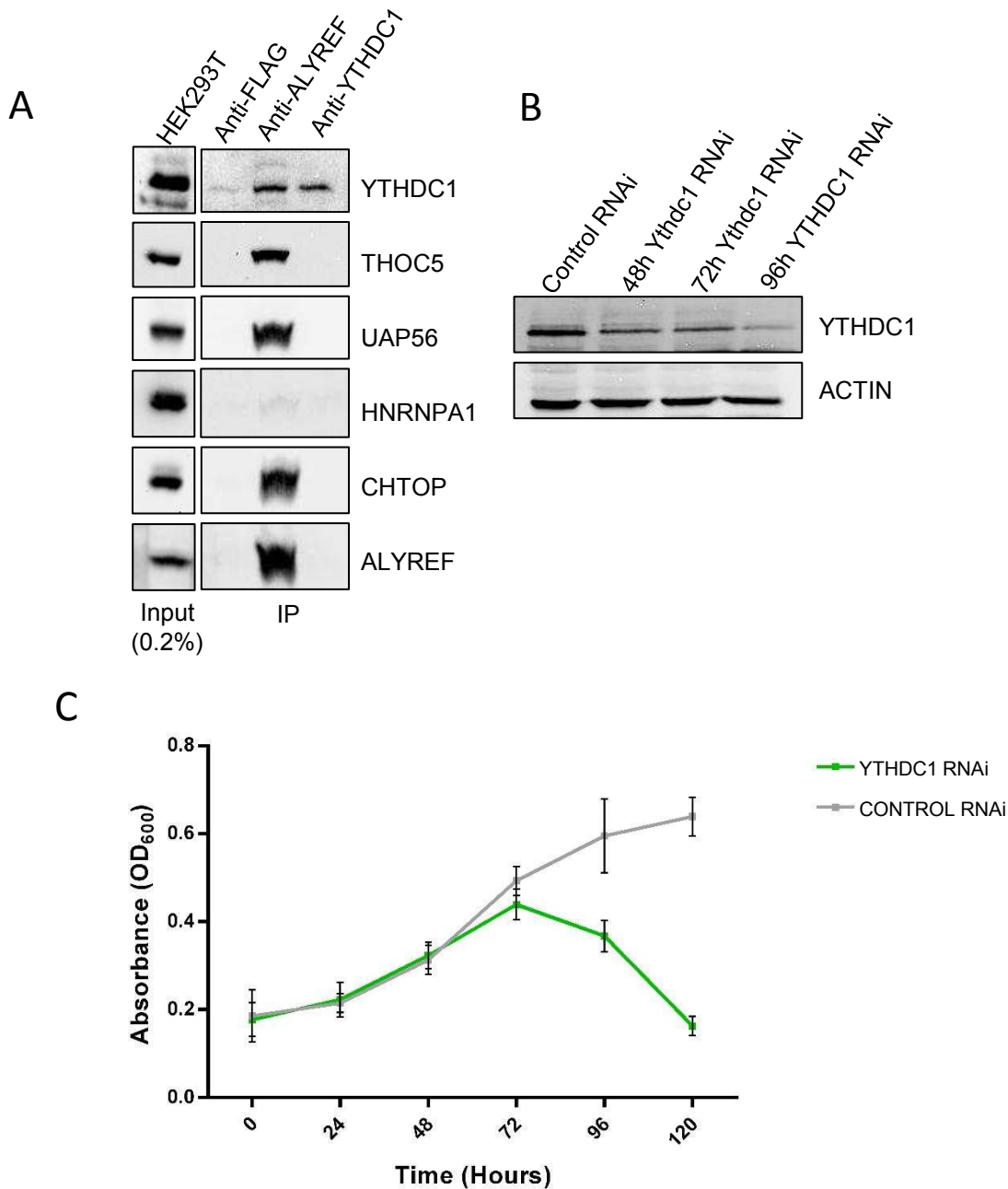
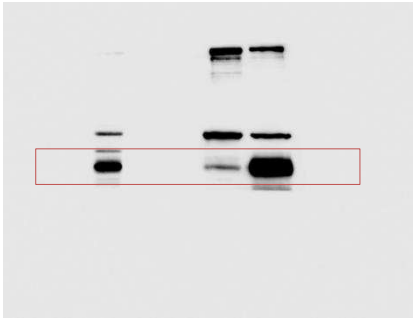


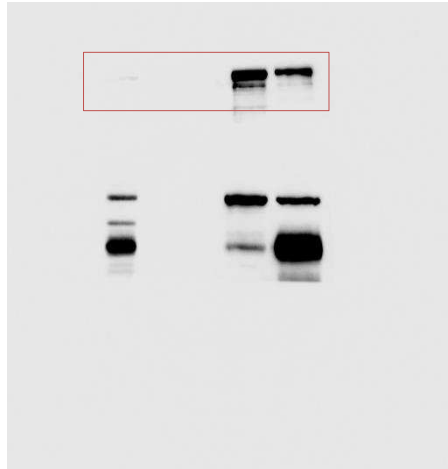
Figure S5. Analysis of YTHDC1. A) Co-IP western analysis for ALYREF and YTHDC1 with the indicated antibodies. B) Western blot analysis of the control and YTHDC1 stable inducible RNAi cell line. The length of time of tetracycline induction of the control or YTHDC1 hairpin is indicated. C) MTT cell proliferation assay was used to follow growth of the stable inducible RNAi cell line following tetracycline induction of the RNAi hairpin for the indicated times. The results represent the average of 3 independent experiments and the standard deviation of the mean is presented. Where separate panels are shown for the same protein in Fig. S4A, the panels were taken from the same blot at the same exposure.

Original images of blots displayed in Fig 1A.
Regions used for Figures are boxed in red

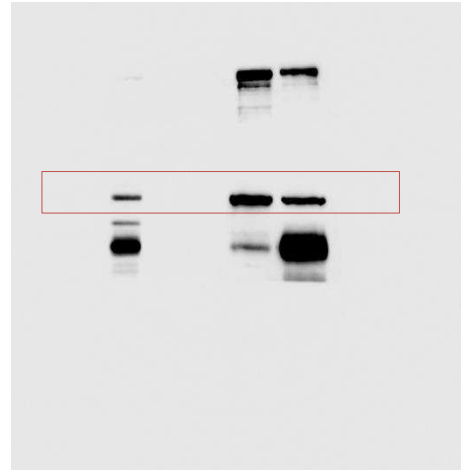
WTAP



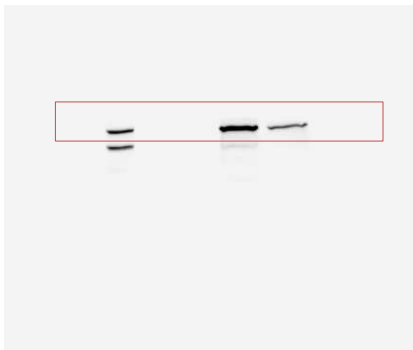
KIAA1429



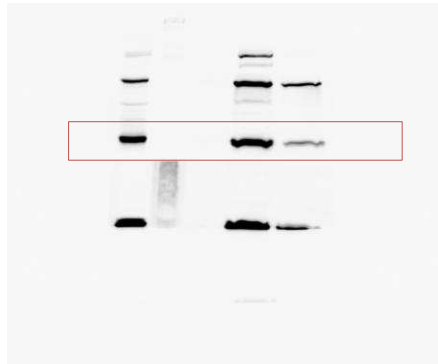
METTL3



THOC5



DDX39A/B



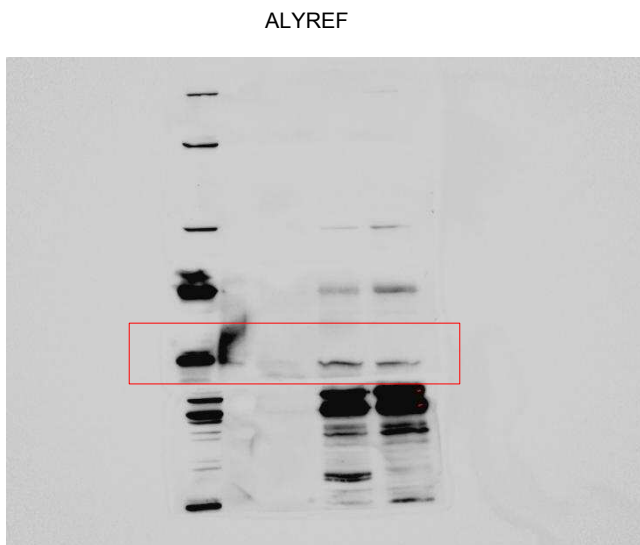
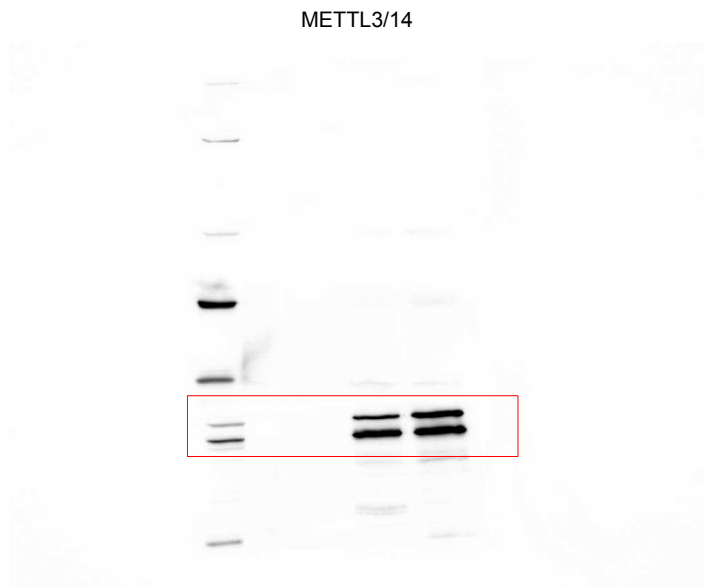
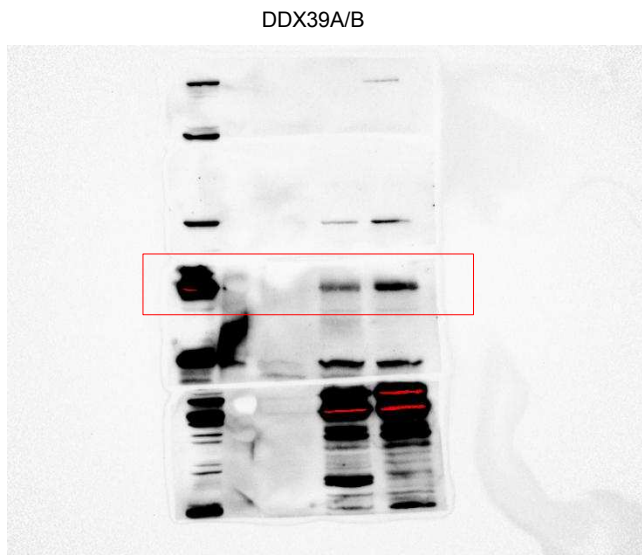
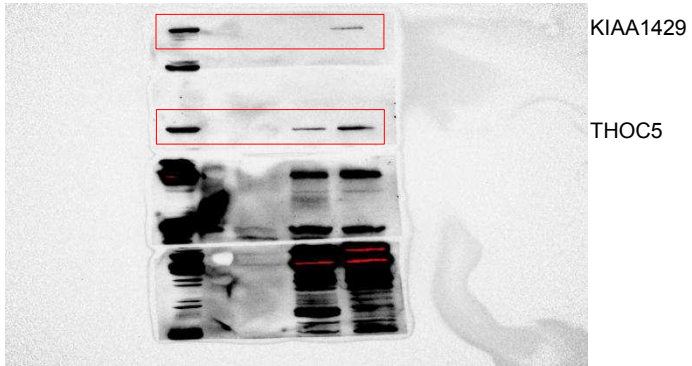
ALYREF



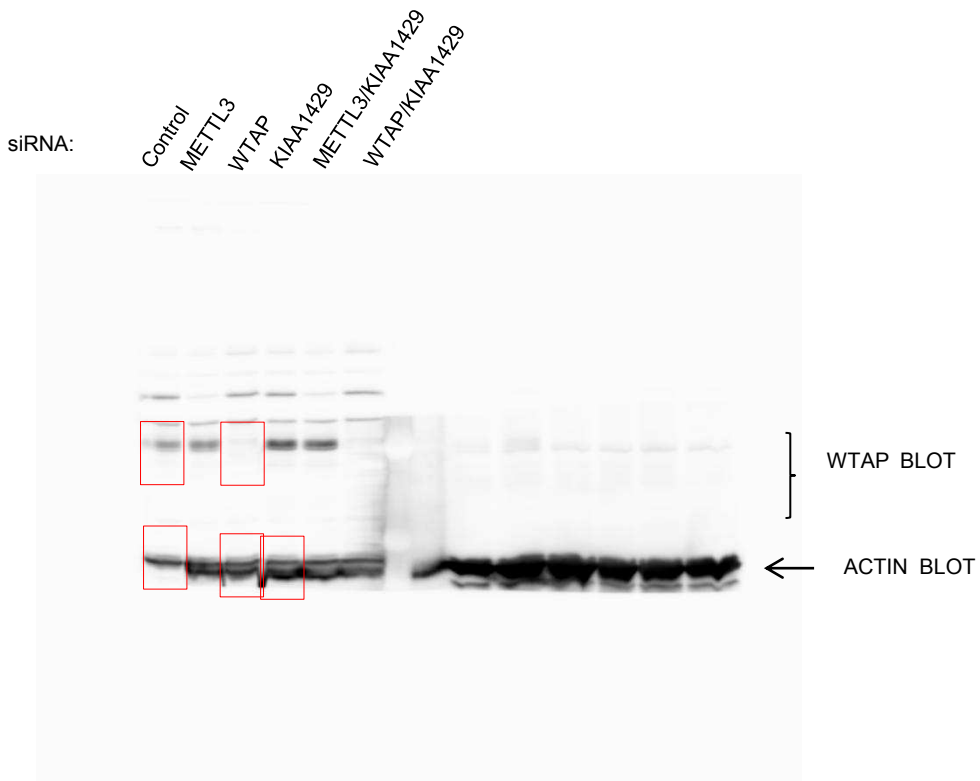
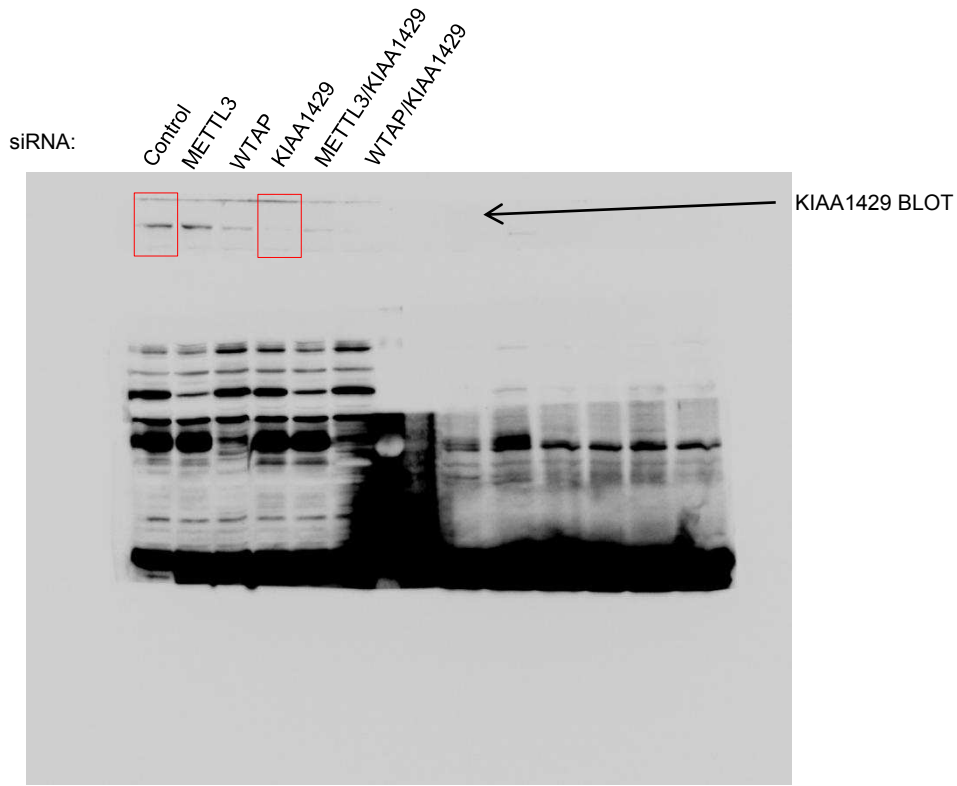
HNRNPA1



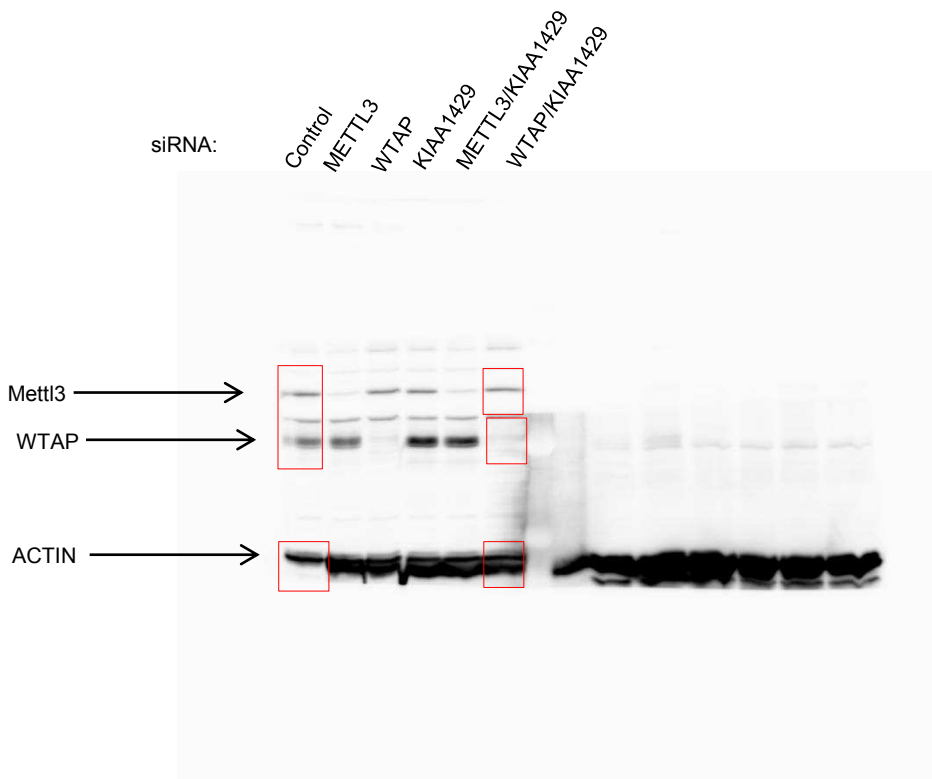
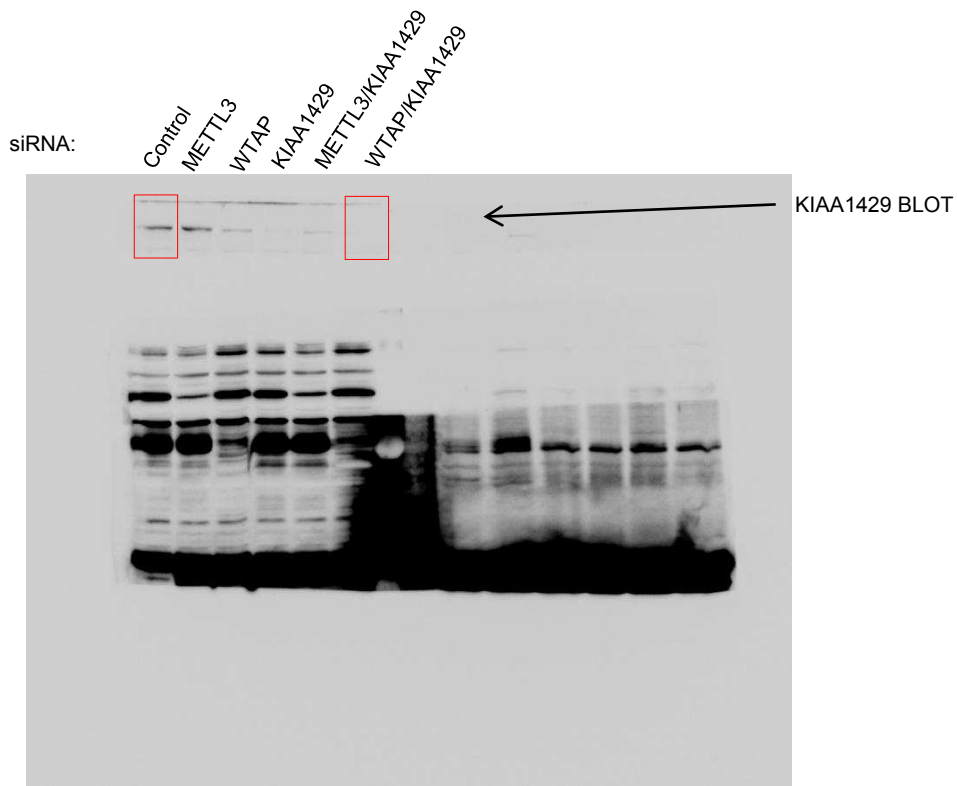
Original images of blots displayed in Fig 1B.



Original images of blots displayed in Fig 1C (upper panel) and S2A.

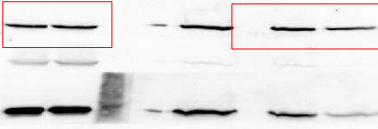


Original images of blots displayed in Fig 1C -lower panel.

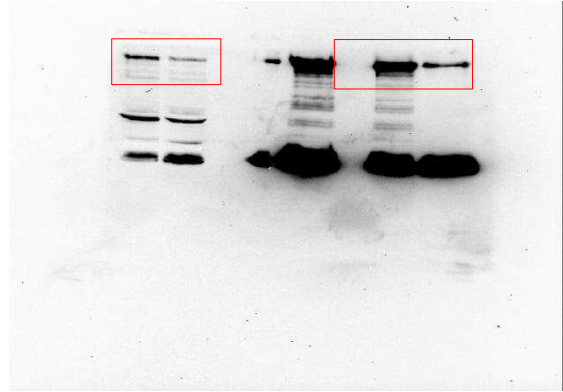


Original images of blots displayed in Fig 1D.

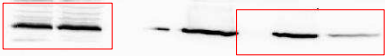
THOC5



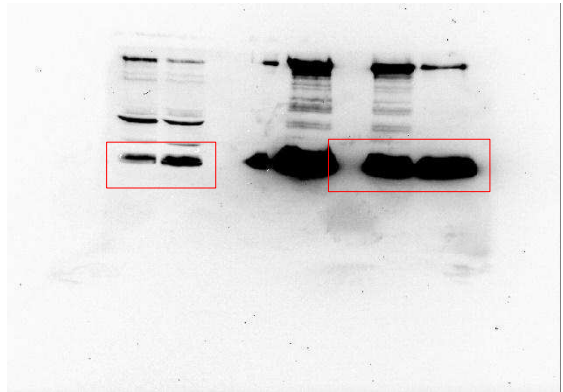
KIAA1429



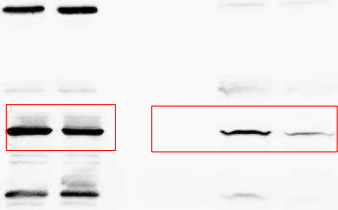
METTL3



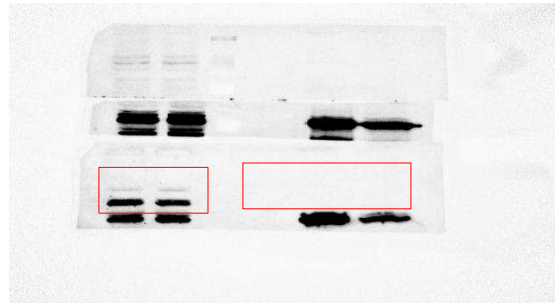
WTAP



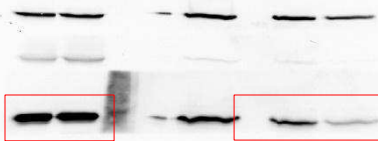
DDX39A/B



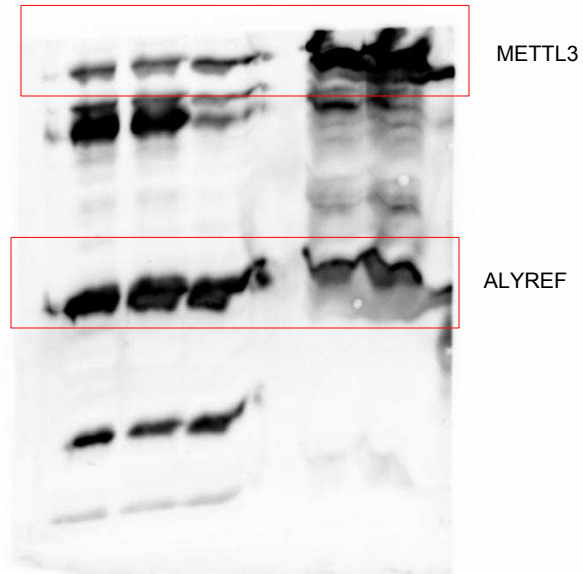
HNRNPA1



ALYREF

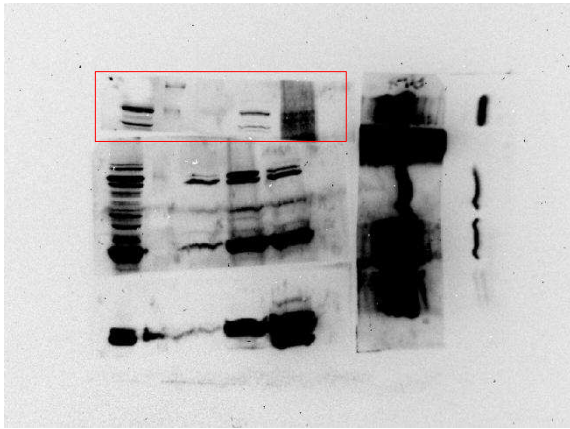


Original images of blots displayed in Fig 1E.

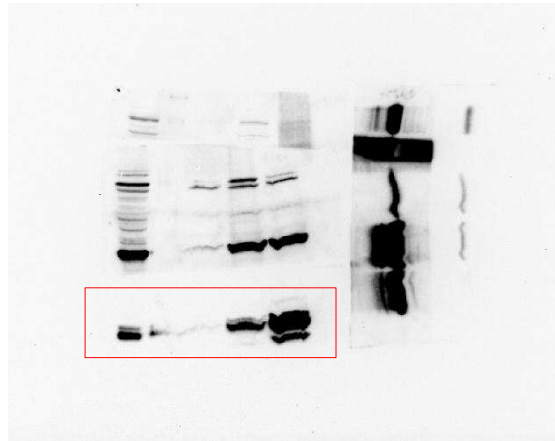


Original images of blots displayed in Fig 5B.

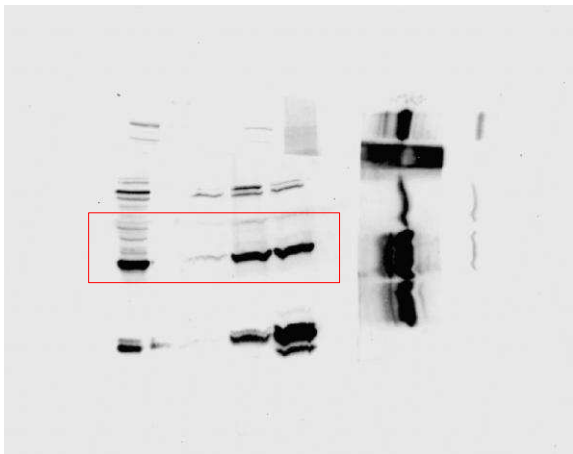
YTHDC1



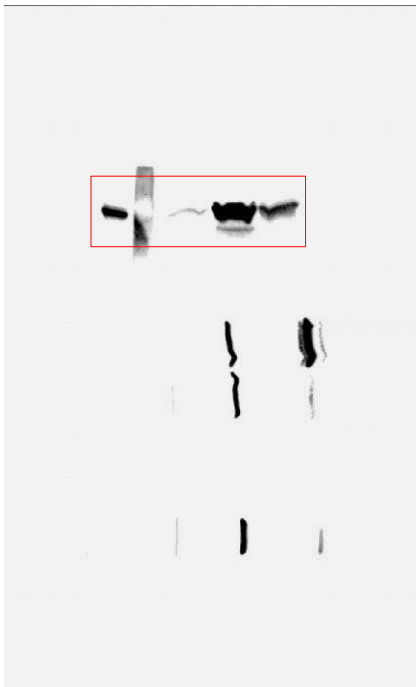
CHTOP



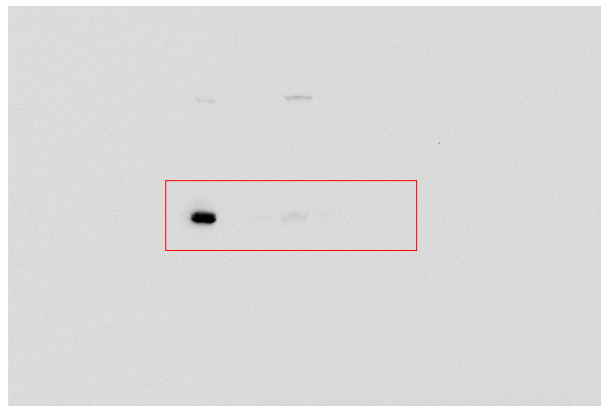
DDX39A/B



ALYREF

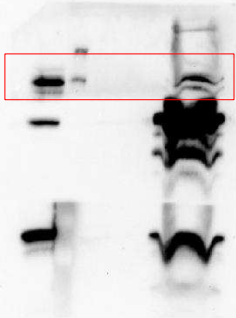


HNRNPA1



Original images of blots displayed in Fig 5C.

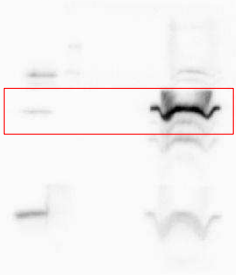
YTHDC1



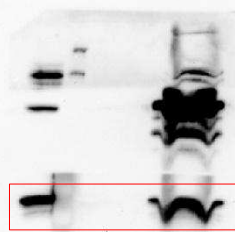
DDX39A/B



NXF1

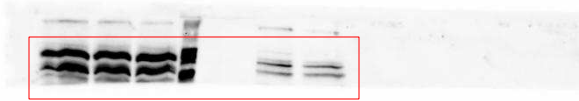


ALYREF



Original images of blots displayed in Fig 5D.

YTHDC1

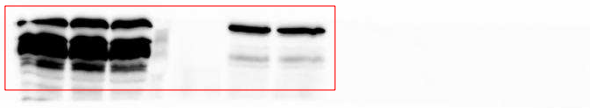


WTAP



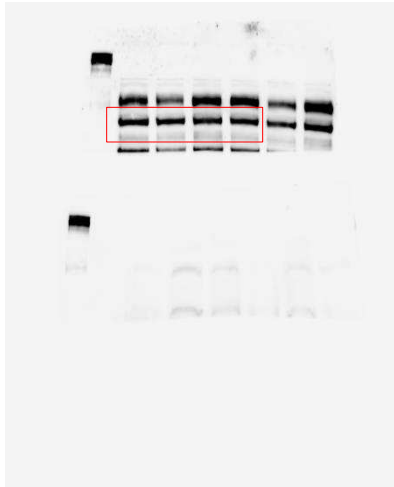
METTL3

METTL14

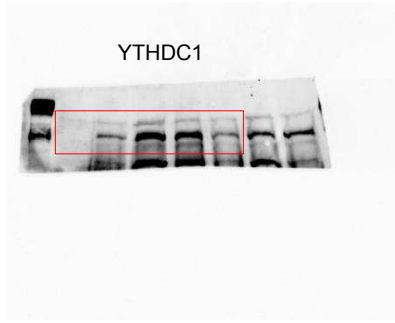


Original images of blots displayed in Fig 5E.

YTHDC1

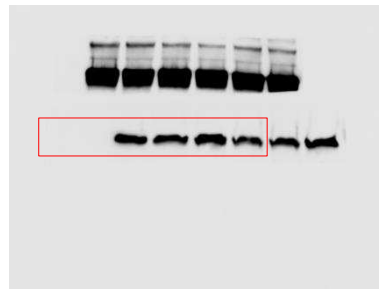
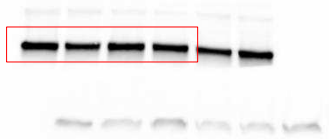


YTHDC1

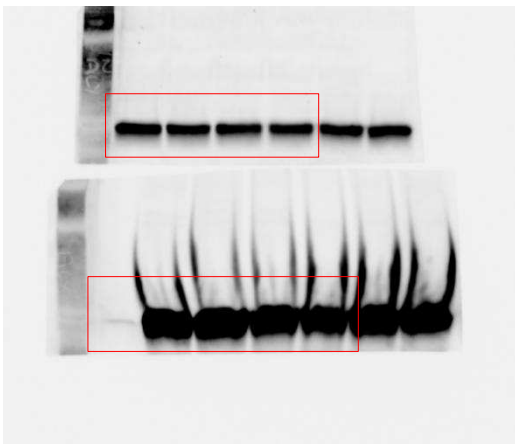


DDX39A/B

DDX39A/B

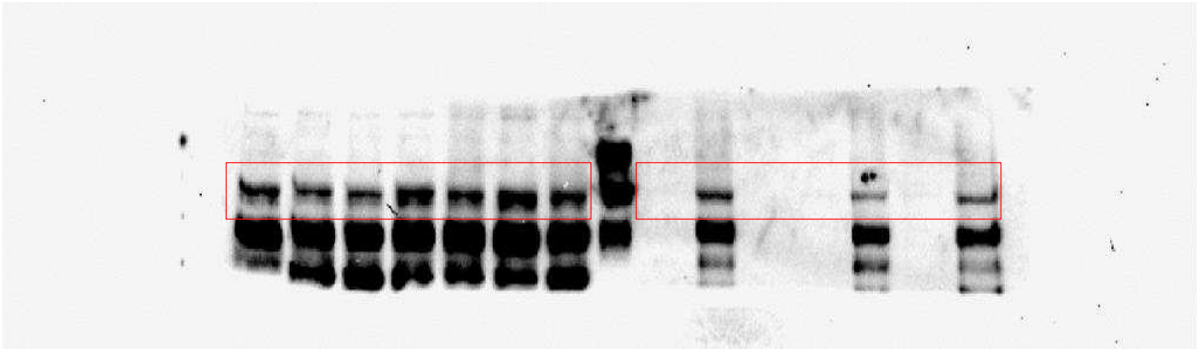


ALYREF

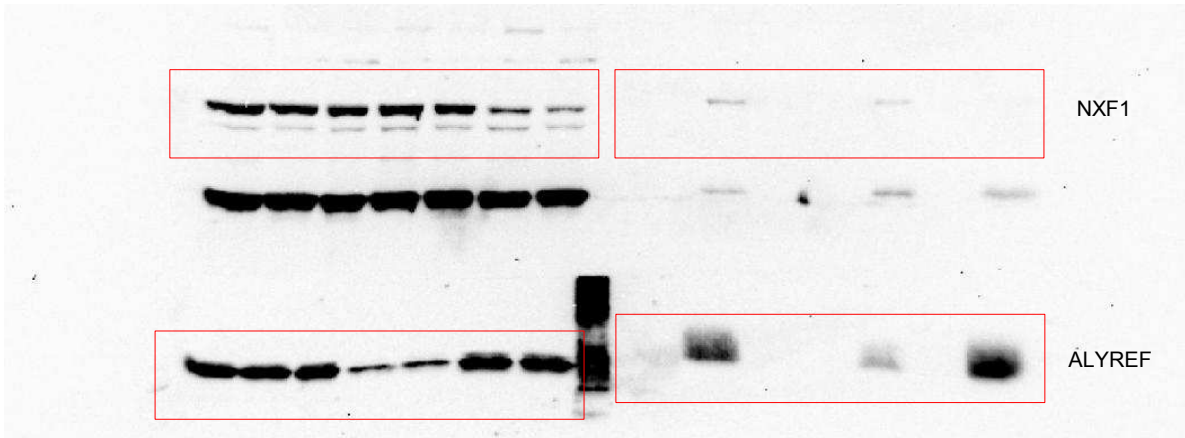
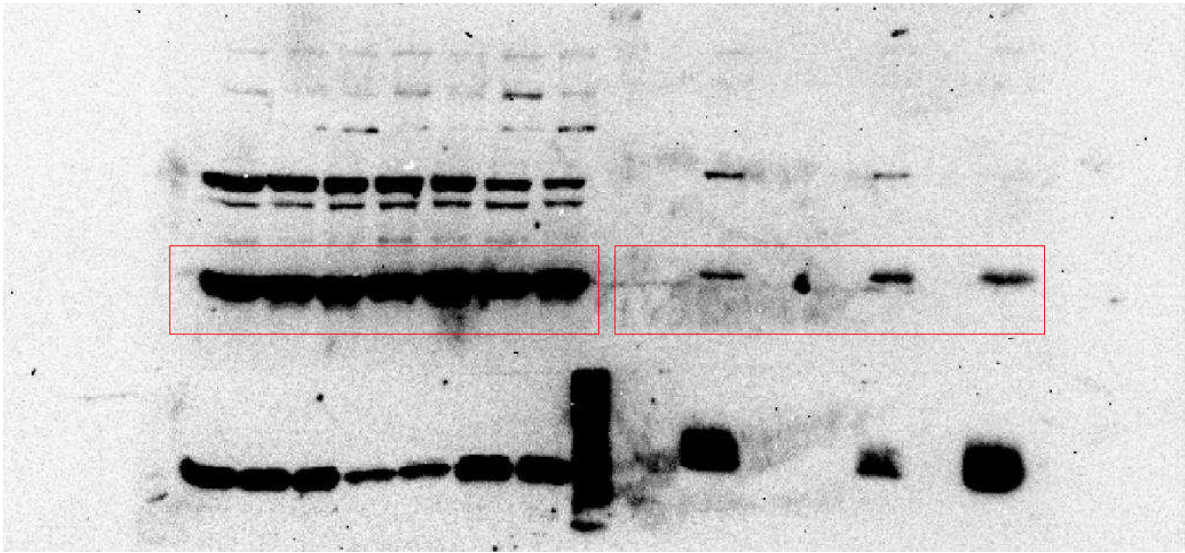


Original images of blots displayed in Fig 5F.

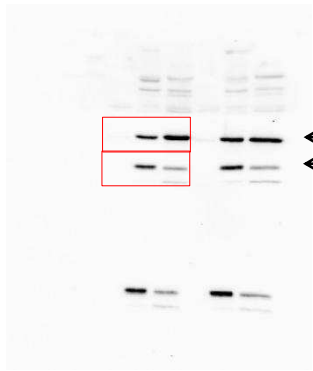
YTHDC1



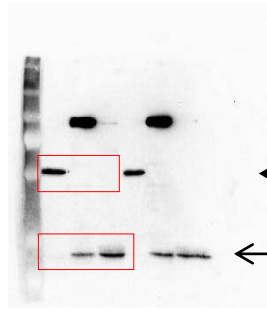
DDX39A/B



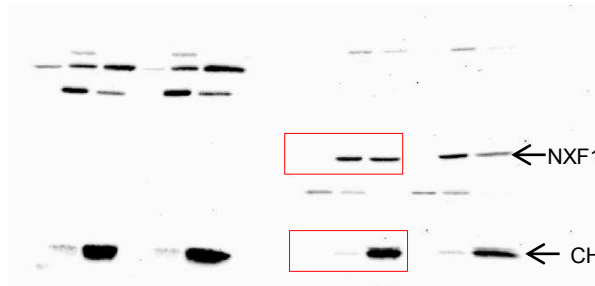
Original images of blots displayed in Fig S1A.



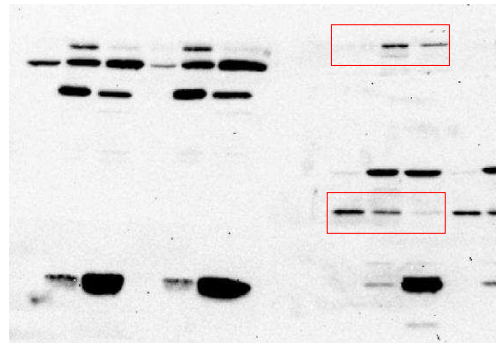
← THOC5 BLOT
← WTAP BLOT



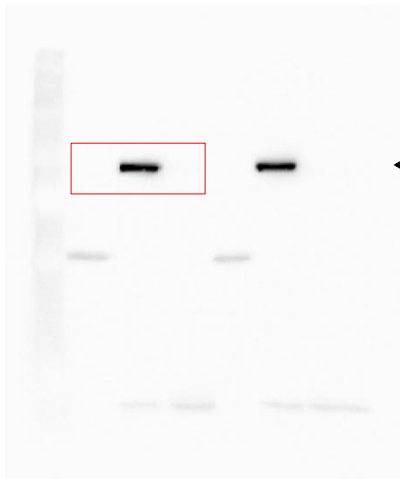
← TUBULIN BLOT
← ALYREF BLOT



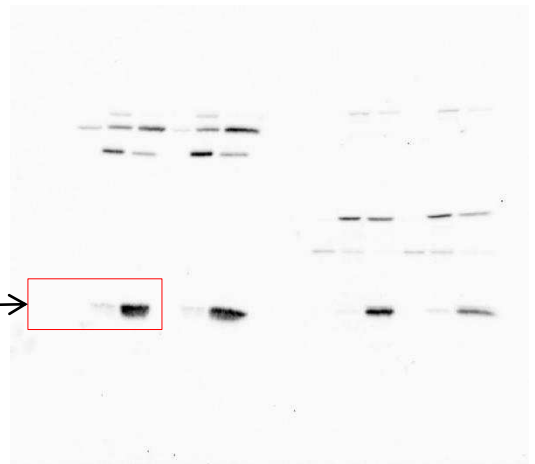
← NXF1 BLOT
← CHTOP BLOT



KIAA1429 BLOT
← METTL3 BLOT

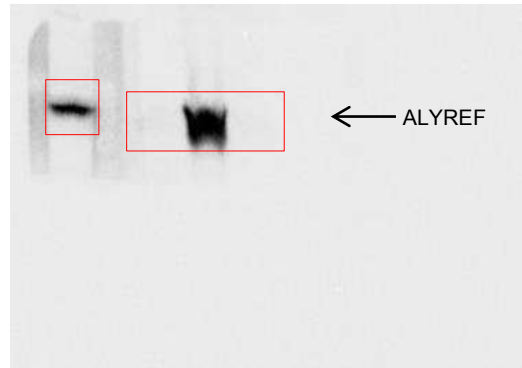
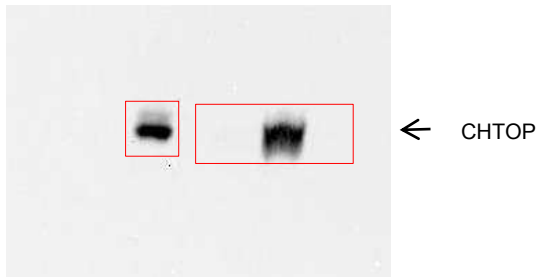
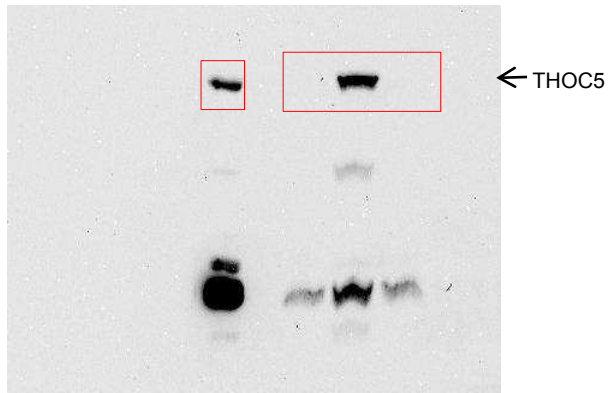
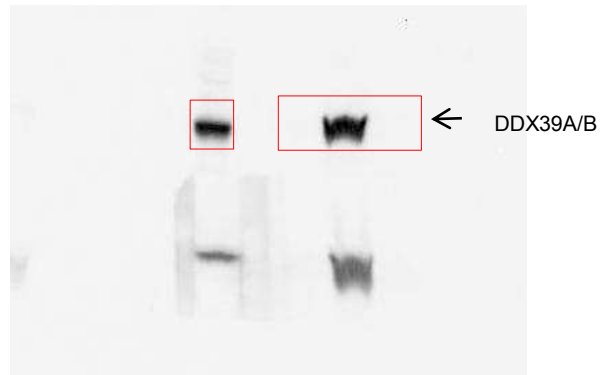
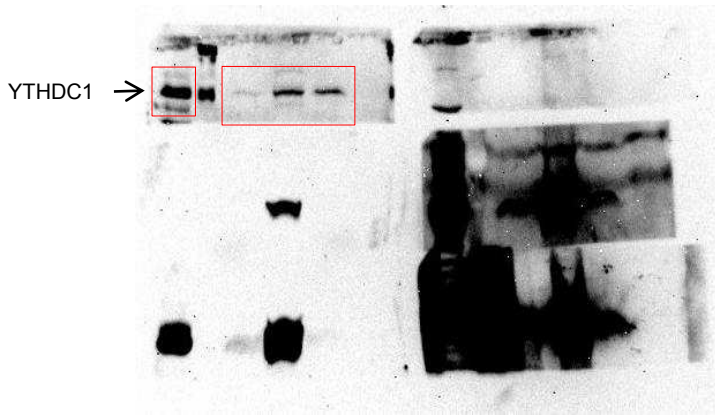


← SSRP1 BLOT



HISTONE H3 BLOT →

Original images of blots displayed in Fig S5A.



Original images of blots displayed in Fig S5B.

